POLITECNICO DI TORINO
Repository ISTITUZIONALE

Creep behaviour of two-component grout and interaction with segmental lining in tunnelling

Original
Creep behaviour of two-component grout and interaction with segmental lining in tunnelling / Oggeri, C., Oreste, P., Spagnoli, G.. - In: TUNNELLING AND UNDERGROUND SPACE TECHNOLOGY. - ISSN 0886-7798. - STAMPA. - 119:(2022). [10.1016/j.tust.2021.104216]

Availability:
This version is available at: 11583/2931553 since: 2021-10-14T17:57:17Z

Publisher:
Elsevier

Published
DOI:10.1016/j.tust.2021.104216

Terms of use:

This article is made available under terms and conditions as specified in the corresponding bibliographic description in the repository

Publisher copyright
Elsevier postprint/Author's Accepted Manuscript

© 2022. This manuscript version is made available under the CC-BY-NC-ND 4.0 license
http://creativecommons.org/licenses/by-nc-nd/4.0/.The final authenticated version is available online at:
http://dx.doi.org/10.1016/j.tust.2021.104216

(Article begins on next page)

14 September 2026

Creep behaviour of two-component grout and interaction with segmental lining in tunnelling

Claudio Oggeri[1], Pierpaolo Oreste[1], Giovanni Spagnoli[2]*

[1] Department of Environment, Land and Infrastructure Engineering, Politecnico di Torino, Corso Duca Degli Abruzzi 24, 10129 Torino, Italy

[2] MBCC Group, Dr-Albert-Frank-Strasse 32, 83308 Trostberg, Germany, Tel: +49 8621 86-3702, *giovanni.spagnoli@mbcc-group.com* ORCID: 0000-0002-1866-4345 (CORRESPONDING AUTHOR)

Abstract

The complexity of the two-component grout behavior significantly affects the interaction between the support system and the tunnel. The loading of the filling material (and also of the segmental lining) takes place during the curing phase. At the end of it a creep phase develops which shows secondary deformations over time which result in a relaxation of the segmental lining and an increase in the deformation of the tunnel wall. In this work, a laboratory experiment campaign allowed to study the two-component material in detail during the creep phase. The typical trend of deformations over time, obtained for different stress load values and material curing age, was identified. The maximum stress was also evaluated which still allows to avoid the failure of the material over time, when a persistent state of stress is applied. The information obtained from the experimentation allowed to provide considerations on the support system-tunnel interaction, using the convergence-confinement method. The approach followed was then applied to a real case of a tunnel excavated in Northern Italy, for which it was possible to estimate the decrease in the load applied to the support system and the increase in deformations of the tunnel wall due to the creep phenomenon of the two-component material.

Key words: two-component grout; curing age; Tunnel Boring Machine (TBM); convergence-confinement method (CCM); creep-behaviour.

Abbreviations and nomenclature

E_{fm} Elastic modulus of the filling material

E_{gr} Elastic modulus of the ground

E_s Secant elastic modulus

E_{sl} Elastic modulus of the segmental lining (concrete)

E_t Tangent elastic modulus

$E_{t,\alpha}$ Tangent elastic modulus of the filling material associated with a percentage load level α referred to the Unconfined Compressive Strength (UCS)

$E_{t,35\%}$ Tangent modulus of elasticity measured at a stress level equal to 35% of UCS

$k_{sys,fin}$ Stiffness of the support system at the end of the loading process

k_{sys} Stiffness of the support system

$k_{sys,in}$ Stiffness of the support system at the beginning of the loading process

k_{sl} Radial stiffness of the segmental lining

k_0 Coefficient of earth pressure at rest

p Pressure inside the tunnel acting on the walls

p_{eq} Final entity of the loads acting on the support system

p_0 Hydrostatic initial stress state (undisturbed)

R Tunnel radius

t_{fm} Thickness of the filling material

t_{sl} Thickness of the segmental lining

UCS Unconfined compressive strength

u_{eq} Final entity of the tunnel wall displacement

u_0 Displacement of the tunnel wall when the support system is installed

u_{max} Maximum displacement of the tunnel wall in the absence of supports

ν_{fm} Poisson's ratio of the filling material

ν_{gr} Poisson's ratio of the soil or rock present around the tunnel

ν_{sl} Poisson's ratio of the concrete constituting the segmental lining

α Percentage of the stress level acting in the filling material with respect to the UCS strength

δ_{inst} Immediate displacement in the filling material

ε strain (ratio of the the displacement on the reference height)

ε_{creep} creep strain of the filling material

ε_{inst} Immediate deformation of the filling material

η Long-term strength of the two-component material as a percentage of the UCS

ω Correction coefficient taking into account the deformation increase that occurs in the first 10 minutes of load during a creep test

σ Applied or induced stress

Δu	Increase in the radial displacement of the tunnel wall due to the creep phenomenon of the filling material

Introduction

The backfilling (or tail void grouting) is the system used during the excavation of a tunnel by means of a TBM (Tunnel Boring machine) to fill the void created during the advancement of the machine between the support structure and the rock wall. As a matter of fact, when tunneling is carried out using a shield machine and a segmental lining, there is a gap caused by the overcut due to the slightly larger diameter of the shield machine than the lining (Sharghi et al., 2018) and to the thickness of the shield and the space occupied by the brushed, which close the void lining-shield (see Fig. 1). This gap is needed in order for the TBM to curve left/right (planimetric curves) or up/down (altimetric curves).

The instantaneous filling of the annulus that is created behind the segment lining at the end of the TBM tail during its advancement is a very important operation. The objective is to minimize the surface settlements induced by the passage of the TBM, to assure that the tunnel convergence is within the allowable limit, to ensure the homogeneous transmission of stresses between the soil/rock mass and the lining, to avoid misalignments of the linings and to provide impermeabilization of the tunnel (Thewes and Budach, 2009; Di Giulio et al., 2020; Oggeri et al., 2021). Different types of materials are used to fill the gap, however lately the two-component grout system is becoming more popular (e.g. Di Giulio et al., 2020; Oggeri et al., 2021; Rahmati et al., 2021). To correctly achieve this, a simultaneous backfilling system and the injected material should satisfy the technical, operational and performance characteristics: the two-component grout must be water-tight, pumpable, workable, able to fill the void, to stiff quickly and to be wash-out resistant, not able to shrink (e.g. Thewes and Budach, 2009; Oggeri et al., 2021).

For these reasons, the open space must be continuously filled during the machine's advancement.

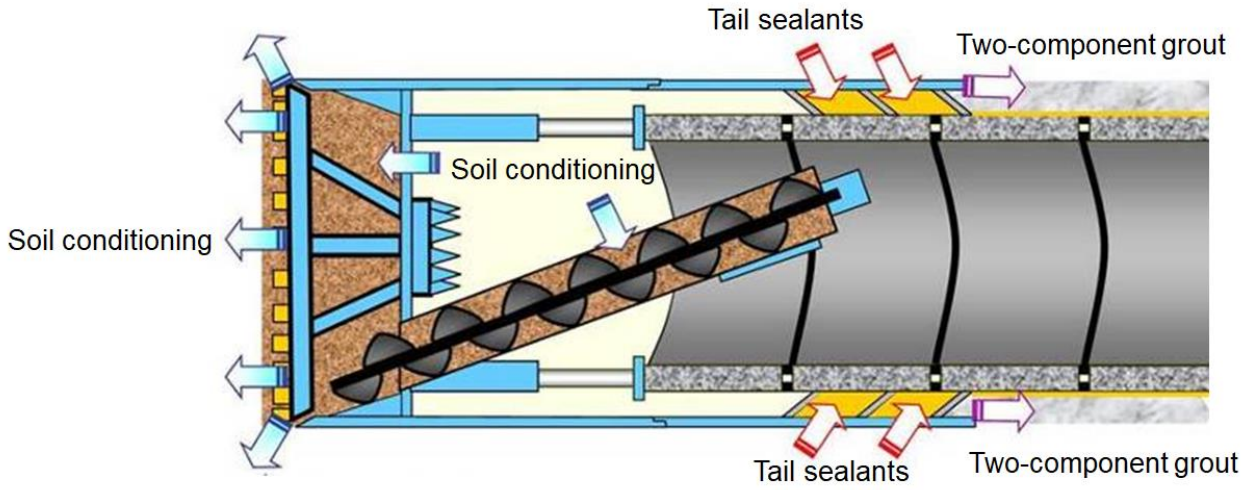

Fig. 1 Section of EPB-TBM with some main aspects highlighted

The mix-design of a two-component grout is claiming for different requirements depending on the job site characteristics and geological formation; however, the typical mix-design in a m^3 system for a two-component grout consists in general by cement (280-450 kg), bentonite (30-60 kg), water (730-860 kg), retarder (3-5 kg) and accelerator (60-80 kg)**,** normally sodium silicate. The accelerator ("B" component) is generally added just before the pumping phase of the mix of water, bentonite, retarder and cement ("A" component). Simultaneous backfilling with two-component grouts, in comparison with the mortar type grouts, keeps in general lower settlements during TBM excavation (Hirata, 1989). Keeping in mind the importance of the two-component grout during tunneling advancement, it must be recognized that not many works deal with this material both experimentally and numerically. It is well-known that the mechanical properties of the two-component grout change based on the mix-design type (e.g. Flores, 2015; Todaro et al., 2019).

Oh and Ziegler (2014), Shah et al. (2018), Ochmański et al. (2018) and more recently Ochmański et al. (2021) performed a numerical analysis regarding the effects of the two-component grout on the tunnel settlement. However, the creep behavior of two-component grouts has not be analyzed in details so far. In this paper, a mix-design of a two-component grout has been tested by determining the Unconfined Compressive Strength (UCS) and the

creep strain evolution at varying curing ages. From the analysis of the laboratory results it was possible to understand the behavior of this material with particular attention to the deformability and strength values during a loading phase and the analogous response to long term loading, by maintaining different loads acting on the specimen. It was possible to describe the development of deformations over time of the two-component material subjected to different load entities related to the UCS. From the analysis of the laboratory results it was possible to describe a behavioral model of the creep phase of the two-component material and also to evaluate the effects of the evolution of deformations over time on the behavior of the segmental lining and on the displacements of the tunnel wall. The analysis of a real case of a tunnel excavated in Northern Italy in a weakly cohesive material allowed to verify the effects of the creep of the two-component material on the behavior of the support system, arriving at evaluating the reduction over time of the loads applied to the segmental lining (stress relief) and the increase in the radial displacement of the tunnel wall at the end of the creep phase.

General creep models

Due to the strains increase with time in tunnelling, creep can be an important phenomenon, especially for very soft or heavily fractured rocks under significant in-situ stresses (Yu, 1998; Dusseault and Fordham, 1993), for rocks of argillaceous nature (Barla, 2011) or also when a combination of applied stresses and material properties, some specific geological conditions, and/or a groundwater flow exist. For rocks containing clay, the phenomenon, associated with water migration (or clay platelets orientation), could be considered as a consolidation typology (Goodman, 1980).

When a specimen is subjected to a constant maintained load in unconfined compression in the microfracturing range, the specimen will continue to deform after initial application of the load (Hardy et al., 1969). Normally creep strain are not fully recovered; therefore, large

plastic deformations take place (Dusseault and Fordham, 1993). Time dependent strain is much higher in weak rocks and evaporites than in stiffer rocks, but the typical shape of the strain trend is similar. Three reference types of deformation can be observed following the strain trend under a maintained stress (Farmer and Gilbert, 1981):

a) level of applied load is maintained above a critical microcrack development level, then unstable fractures will accelerate creep strains and quickly leading to specimen failure;

b) level of stress is well below the critical microcrack development level, there will be a limited spreading of fractures with an exponentially decaying of the creep strain rate and stable conditions (no failure);

c) the intermediate zone represents a meta-stable condition, where cracks propagation can occur leaving stable microfractures and reaching unstable conditions with crack acceleration and failure. This can happen also with staged conditions of loading (Figure 2, Oggeri, unpublished data).

Figure 2 shows an example of evaporitic rock presented for comparison with different behaviour with deformation under constant loading. Trend of the curves, threshold levels for both stress and strain and final control of specimen integrity can differ during testing. Therefore, a dedicated experimental approach is deemed necessary for any new material. Specimen a) and b) are coming from the same deposit, but even small differences in texture and grain size of particles are influencing the test results.

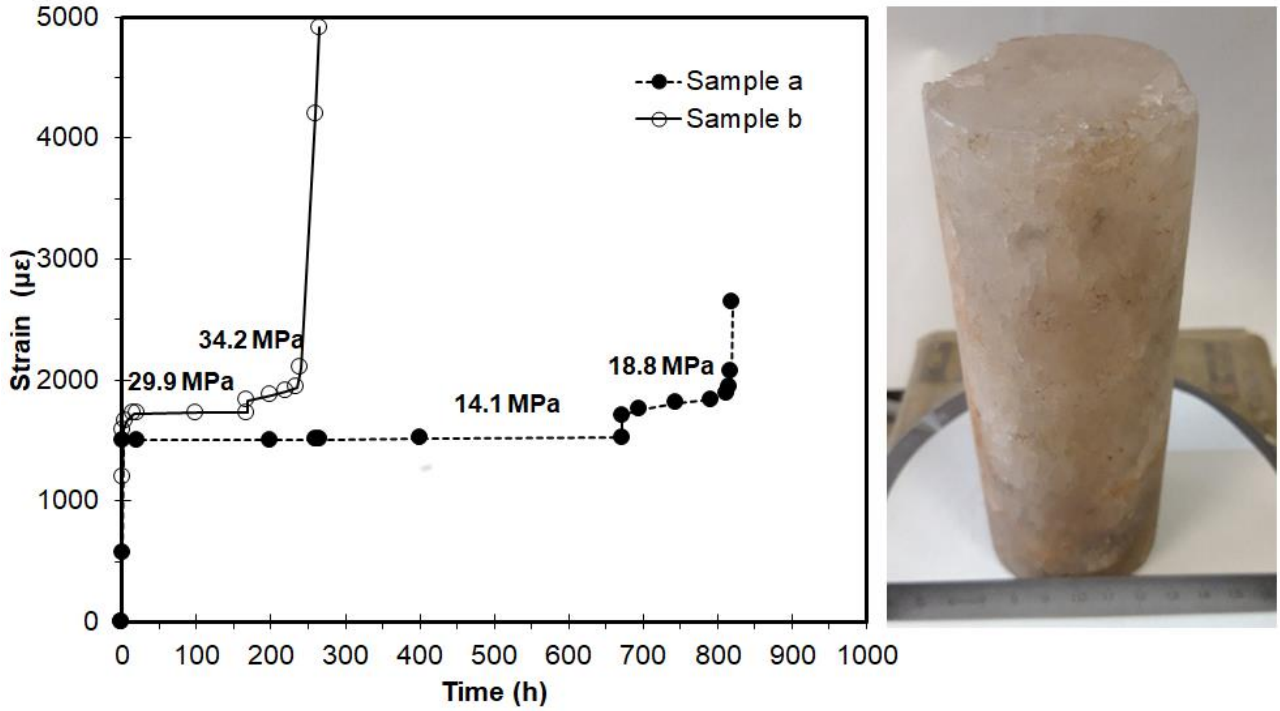

Fig. 2: Two examples of creep with a staged loading on evaporitic rocks. Specimen a) is entirely made of salt, with microcrystals from millimetric to centimetric size (see figure on the right); after an initial stable load at 14.1 MPa, failure is reached with a step at 18.8 MPa. Specimen b) is a fine-grained salt including elements of marl; after an initial load at 29.9 MPa, failure is reached with a step at 34.2 MPa.

Many models of creep and testing procedures have been carried out after the extended research by Griggs (1939) and refinements after Lama and Vutukuri (1978). Alternative approaches have been developed by Price and Farmer (1981).

In tunneling, many models are used to describe the creep of rocks and sprayed concrete, e.g. rheological models (Jaeger and Cook, 1979), Kelvin model (Neville et al. 1983; Jaeger and Cook, 1979; Rokahr and Lux 1987), Burgers model (Yin 1996), viscoplastic model (Thomas 2009). In sprayed concrete creep is significantly higher at an early stage of load as the strength of sprayed concrete is lower, as found by Huber (1991), who observed that a sample loaded at 8 days creeps by 25% more than a similar sample loaded at 28 days.

However, it must be kept in mind that some accelerators increase the early strengths (Melbye 1994) therefore creep after 24 or 48 h is close to that at greater ages (Kuwajima 1999). Besides, studies have been carried out for the assessment of creep reaction of grout for rockbolts (Van der Schyff, 2007), or for a new method for designing the grout mix based on the induced shear stress rather than on the compressive strength (Orumchi and Mojallal, 2017); other contributions have been given for the creep behavior of a grouted sand (Delfosse-Ribey et al., 2006): depending on the nature of the grout, the grouted sand has exhibited creep strains of different degrees; moreover, similarities can be found for both creep behavior and fatigue behavior as found trend curves have shoved similar shapes.

Arnau et al. (2011) provided analyses in order to study the backfill grout behavior and its influence on the longitudinal response of the lining in plane strain. Three different grout moduli of elasticity were used in the analysis for each different ground condition. An assessment of the influence of grout shrinkage was also performed by assuming a value of 0.05 mm/m according to favorable curing conditions. The results showed that the modulus of elasticity of the grout was not presenting a significant influence on the lining axial stress, while tensile cracking for very stiff grouts could occur and that the lining creep and the grout shrinkage were not significantly influencing the grout tensile stress for general tunnel conditions. Backfill grout cracking was unable to influence negatively the radial structural capacity of the segmental lining, while caused a reduction in the water-tightness of the lining. It must be pointed out that in some cases (hydraulic tunnels) there is a significant internal pressure in the tunnel which forces the backfilling mortar to play a crucial role of contact between lining and rock mass. Besides, over time cracks lead to a loss of confinement of the same backfilling material which, consequently, significantly reduces its mechanical characteristics which could also lead to significant alignment/structural problems in the lining.

As final comment, the annulus grout material may remind of clay (bentonite)-cement slurries for diaphragm wall applications (e.g. Cardu and Oreste, 2012; Spagnoli et al., 2016). Although creep behavior may be studied, operative care is focused mainly on integrity, low permeability performances, self-sealing properties, as well local displacement of the structure *in situ*. For the annulus grout loading values are changing together with curing, and stiffness and time performance is governing the interaction between a soft material (usually the ground) and a very stiff material (the concrete segments).

Laboratory creep behavior of the two-component grout

The tested two-component mix-design adopted for this experimental campaign was based on the following parts:

- Part A: water 800 g, bentonite 35 g, cement (CEM I 52.5) 350 g, retarder 17.5 g (solution contains 20% solid therefore retarder dosage by weight of cement is 1%);
- Part B: water glass (sodium silicate) 85 g.

Part B is added at the end of mixing of the mentioned components as it reacts quickly by producing a viscous grout (water glass represents about 7% of added weight to the initial mix). Grout has been prepared starting from the bentonite hydration (duration at least 48 hours), then the slurry has been maintained for another 24 hours at low stirring. The mixing with retarder and cement has been arranged directly inside the casing of the specimens, by manual dispersion; finally, water glass catalyst has been injected into the fluid grout and a high-speed rotating mixer (up to 8000 rpm) has been used during this phase. Every specimen has been prepared by respecting the mass percentages provided for the standard mix; weight of the components has been determined by means of 0.01 g precision scale.

Fast rotation of mixer has allowed to disperse the catalyst and homogenize the grout inside the casing. Then, the casings containing the specimens have been recovered in a box for

curing in water. Curing procedure has been selected following three different timelines for testing: 24 h; 7 days; 28 days. Preparation of the specimen requires great care and repeated preliminary attempts were done in order to obtain a suitable material. Temperature during the tests has been kept constant at 19-21°C.

UCS has been carried out in a Belladonna mechanical press for soils, equipped with bidirectional displacement rate control device. Transducers used to measure load and vertical displacement have been respectively a full bridge load cell (CCT model, full scale 5 kN and precision of 1 N) and LVDT devices (HBM models, precision 0.001 mm). Vertical displacements have been measured following the relative movement of the base of the specimen. Advancing rate has been adapted in the range of 0.15 ÷ 0.45 mm/min and suitable results have been obtained for the range 0.30 ÷ 0.45 mm/min. This selection is a good compromise to avoid creep behavior (excess of lateral swelling) or sudden failure (vertical cracks). Specimen diameter has been selected as 46.5 mm.

Creep testing has been performed by using a standard mechanical oedometer (Belladonna equipment) (Fig. 3), with settings to host the cell (a graduated plastic cylinder) with water and the specimen. The host cell was made of stiff and transparent polypropylene and the contact base with the specimen has been provided of a flat stainless-steel disk to avoid any local deformation. A similar arrangement was already successfully used by Delfosse-Ribey et al. (2006).

The adaptation of a classical Bishop lever oedometer has been done in order to fit the expected strength level of the grout, if compared with typical properties of rock material tested for creep (salt, coal, gypsum etc.). This equipment permits:

- to work from very low to medium stress levels;
- to provide a perfect vertical alignment of caps at the extremities of the specimen;
- to provide a full recovery of mechanical gaps during assembling of specimens;

- an easy water saturation control in open cells and drainage filters at contact with the specimens;
- to continuously read the vertical displacement versus time; easy and direct check of macroscopic cracking growth or lateral bulging.

The procedure for testing is following some steps: 1) preparation of the specimen with selected mix and curing time in submerged conditions; 2) weighting and photos of the specimen; 3) assembling inside the cell and filling of the cell with water; 4) mechanical gap recovery of the displacements of the apparatus; 5) application of the selected load on the lever arm in order to reach the selected stress level, according to previous experience gained in uniaxial compression tests; 6) measurement of vertical displacement versus time; 7) detection of the trend and completion of the testing duration after reaching either a failure (stable failure when residual bearing capacity is evident; unstable failure when specimen start to yield and collapse) or a constant settlement; 8) removal of load and measurement of eventual elastic strain recovery; 9) removal of the specimen, taking photos to verify the crack pattern and weighting for moisture content.

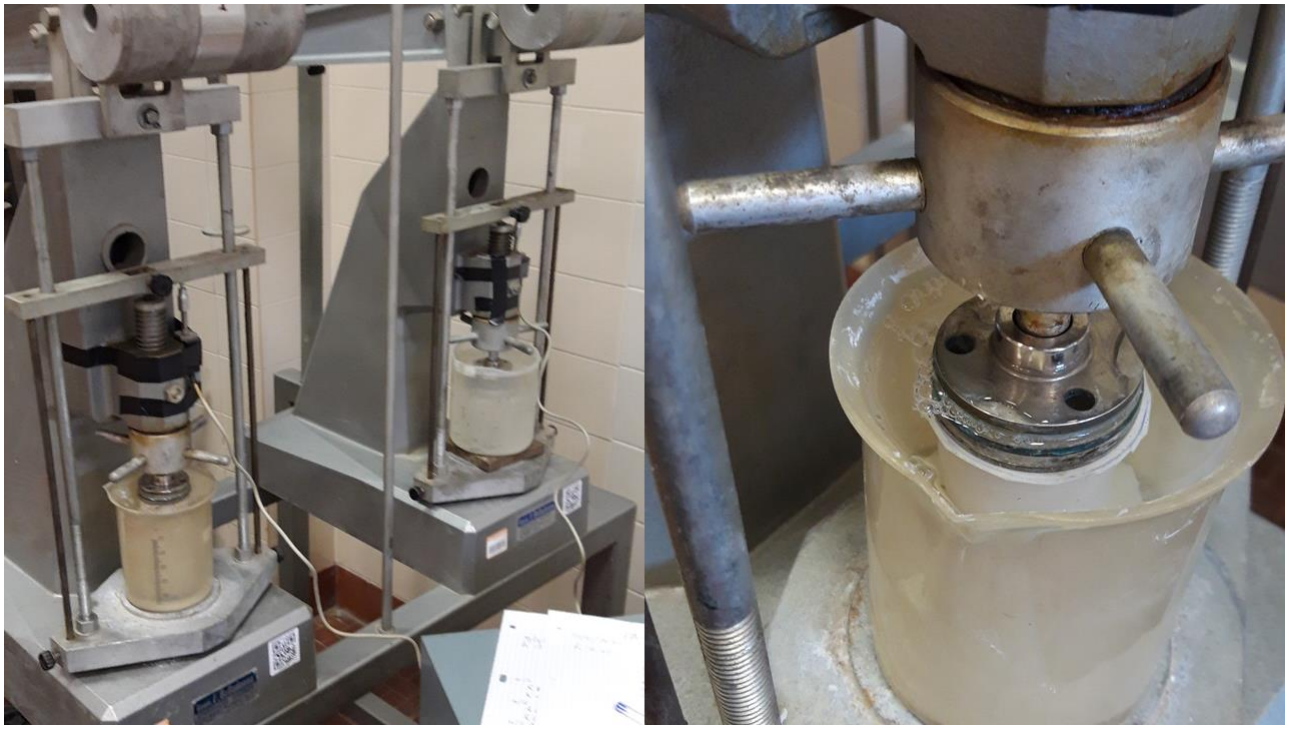

Fig. 3 Left: Twin cells adapted in the oedometer frame, where specimens are kept submerged during constant load application and vertical settlement of the base is continuously measured. Right: detail of a specimen inside a testing cell.

It is important to specify that standard test procedure for one-dimensional consolidation properties of soils have been adapted in order to respect the fact that grout is curing during testing: this is not the case for natural minerals such as salt or gypsum. After some practical preliminary tests, repeatability and representativity have been observed for loading periods of no more than one week after 24 hours of initial curing and of no more than four weeks after 7 days and 28 days form curing beginning. Specimens have been maintained saturated during cycles to avoid cracking, and displacements have been measured by means of potentiometric transducers with precision of 0.01 mm. Fig. 4 shows the specimens used for the tests. Quality in terms of homogeneity and geometry was considered acceptable.

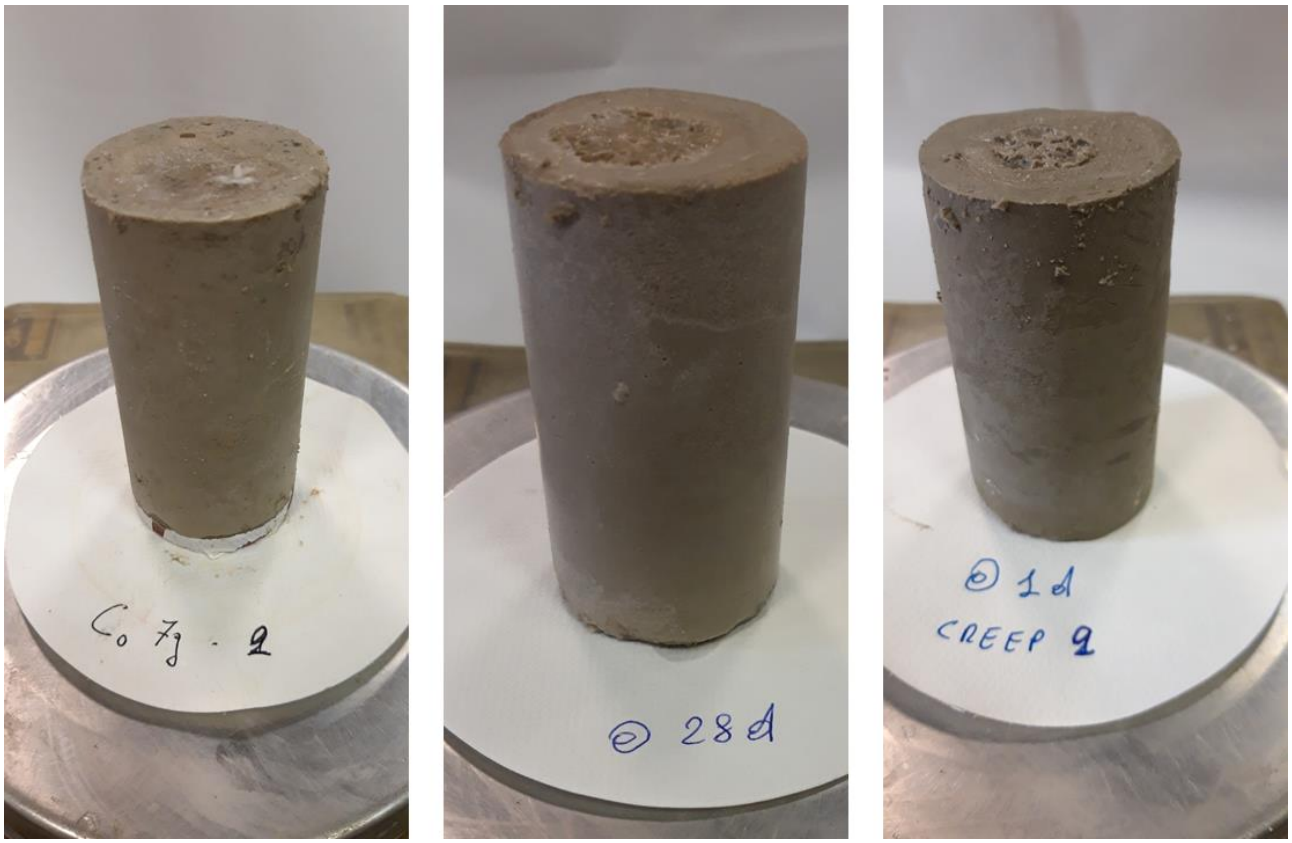

Fig. 4 Example of standard specimens prepared and obtained for UCS and creep testing. The grain size of the cured grout specimens appears regular and homogeneous, without veins or lenses of different consistency.

UCS results

The main results after unconfined compression testing are reported in Table 1. Strength is considered as the maximum value of stress obtained, for the great majority of cases, at yield at the end of the elastic domain. Deformability values are indexed as secant moduli, E_s, at 25%, 50% and 75% of the elastic domain and as tangential values, E_t, at 50% of the elastic domain. In Fig. 5 there is a representative sequence of vertical stress – vertical strain curves for different curing ages. The observed UCS values are rated similar than expected if compared with other available results on this grout type (see Oggeri et al., 2021). Vertical stress versus vertical strain is reliable both in the elastic and in the post peak field. A clear yielding and softening behavior have been observed, with some subvertical and inclined prevailing cracks. In some cases, a pseudo-conical shape at failure has been observed at the extremities of the specimen, thus respecting the ideal Mohr-Coulomb strength criterion (Fig. 6).

291 **Tab. 1 Summary of specimen data for the UCS tests.**

24 h curing	**Diameter (mm)**	**Height (mm)**	**Weight (g)**	**Apparent unit weight (g/cm^3)**	**UCS (kPa)**	**E_s 25% (MPa)**	**E_s 50% (MPa)**	**E_s 75% (MPa)**	**E_t 50% (MPa)**
n.1	46.5	85	187.6	1.299	480	6.5	9.7	11.5	23.1
n.2	46.5	84.4	185.0	1.291	215	5.6	8.7	10.2	17.9
n.3	46.2	85.2	186.2	1.304	350	9	12.3	16.5	26.2
n.4	46.5	84.9	186.3	1.292	320	8.1	10.1	13.3	24.7
7 days curing	**Diameter (mm)**	**Height (mm)**	**Weight (g)**	**Apparent unit weight (g/cm^3)**	**UCS (kPa)**	**E_s 25% (MPa)**	**E_s 50% (MPa)**	**E_s 75% (MPa)**	**E_t 50% (MPa)**
n.1	46.5	86	190.1	1.302	1270	25.8	34.1	42.6	78.1
n.2	46.5	86	192.0	1.314	1110	17.5	26.5	32.3	73.8
n.3	46.5	83	186.3	1.322	760	51.2	63	74.7	76.41
n.4	46.5	84	190.1	1.332	1150	38.5	50	55.4	117.8
n.5	46.5	89	192.6	1.274	990	33.3	43.2	54.6	109.9
28 days curing	**Diameter (mm)**	**Height (mm)**	**Weight (g)**	**Apparent unit weight (g/cm^3)**	**UCS (kPa)**	**E_s 25% (MPa)**	**E_s 50% (MPa)**	**E_s 75% (MPa)**	**E_t 50% (MPa)**
n.1	46.5	83	183.3	1.300	1290	37.8	44.8	54.9	109.4
n.2	46.5	83	185.5	1.316	1110	20.4	26.2	32.7	63.3
n.3	46.5	84	188.6	1.322	1290	33.3	44	59.6	108.7
n.4	46.5	86	192.1	1.315	1400	30.1	43.1	57.1	111.2

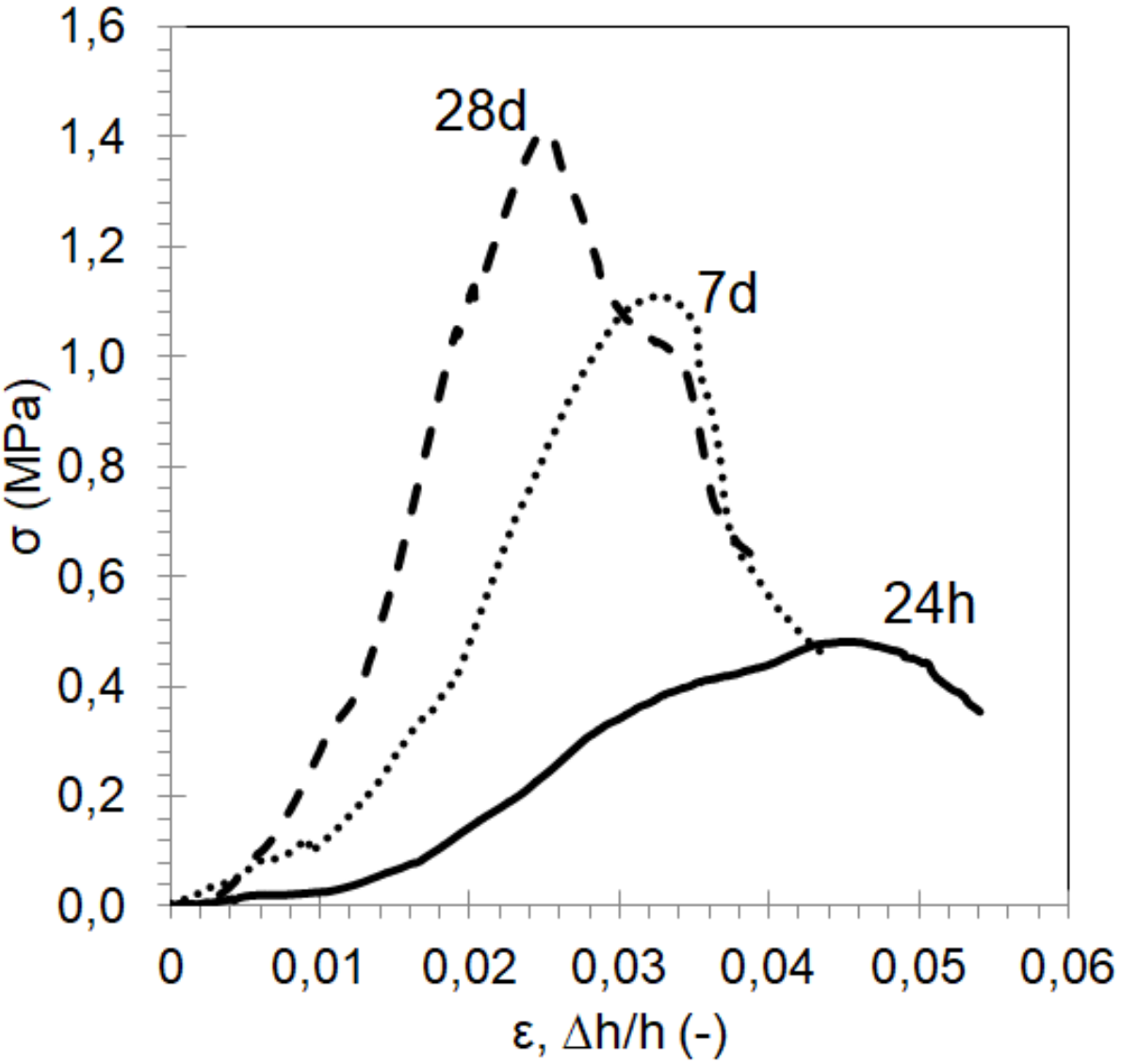

Fig. 5. Examples of vertical stress – vertical strain curves for grout specimens at different curing age (at 24 hours, 7 days and 28 days from curing beginning, respectively), during a uniaxial compressive test. Along the vertical axis applied stress σ in MPa is reported, along horizontal axis induced vertical strain in ε (ratio of the vertical displacement on the sample height) is reported. Strain softening after the stress peak is more evident for short age curing specimens.

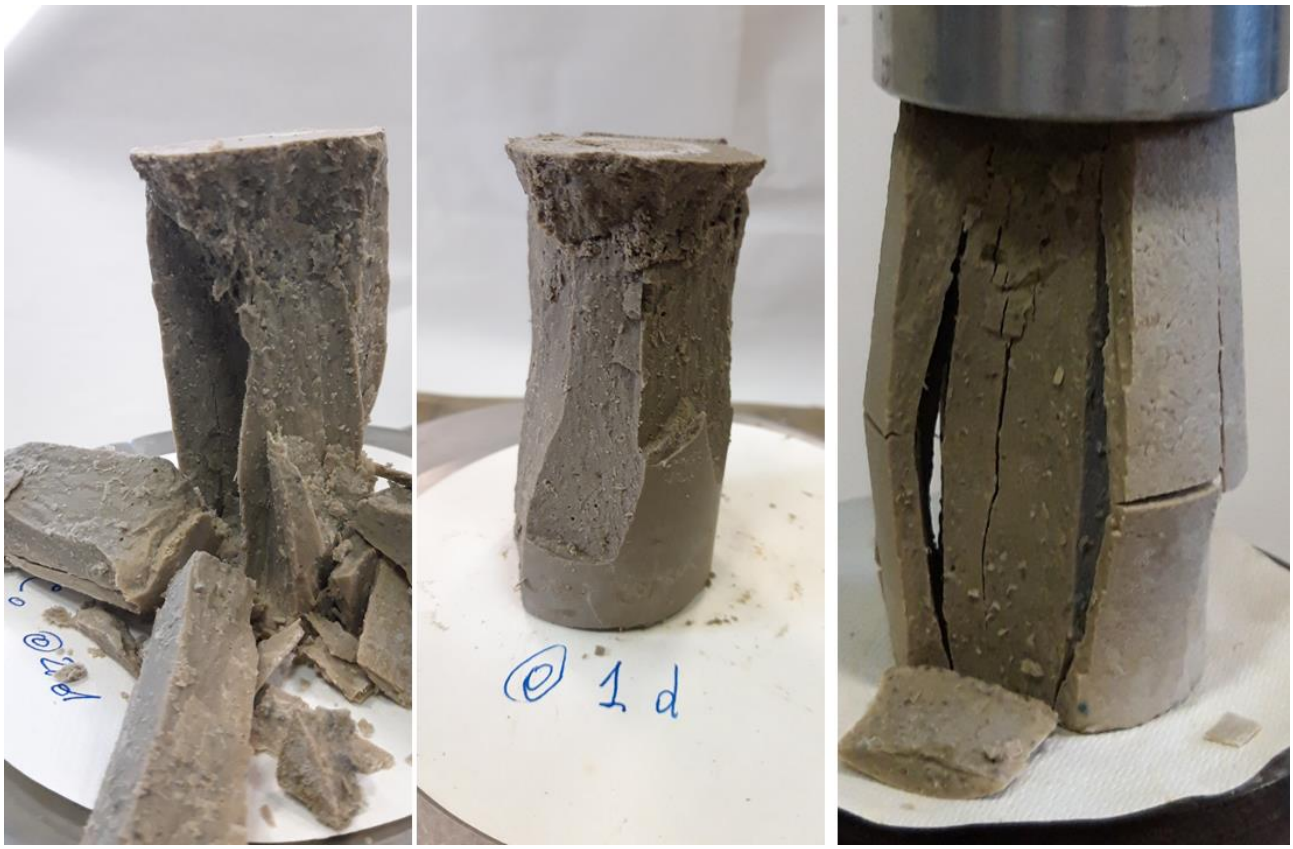

Fig. 6. Different failure modes for specimens after unconfined compression testing. The formation of conical shaped bodies is clearly visible at left and in the middle. On the right, the radial expansion has prevailed with symmetrical formation of vertical slabs.

Creep tests results

Constant loading testing has been carried out on several specimens, and the selection of regular behavior has been reported after exclusion of not homogeneous materials. In Table 2 the evidence of 11 tests is reported, with geometrical data and the applied vertical load**s**, both effective and as a percentage of the reference value obtained from the compression tests. The UCS has been determined in advance in order to properly assign a reasonable ratio of the applied constant load, just because this ratio triggers the passage between a stable and an unstable behavior.

Tab. 2. Summary of specimen data for constant loading (creep) tests. Last column shows the load percentage referred to a representative value of UCS for the same type of grout and curing age.

24 h curing	**diameter (mm)**	**height (mm)**	**weight (g)**	**apparent unit weight (g/cm^3)**	**σ creep (kPa)**	**σ creep (as % UCS)**
n.1 creep	46.2	85.3	187.1	1.308	290	75
n.2 creep	46.5	85.2	186.2	1.287	230	60
n.3 creep	46.5	85.8	187.2	1.285	175	45
n.4 creep	46.5	87.6	189.2	1.270	115	30
7 days curing	**diameter (mm)**	**height (mm)**	**weight (g)**	**apparent unit weight (g/cm^3)**	**σ creep (kPa)**	**σ creep (as % UCS)**
n.1 creep	46.5	87.0	192.0	1.300	700	66
n.2 creep	46.5	85.6	187.9	1.293	580	55
n.3 creep	46.5	93.8	203.8	1.279	460	45
n.4 creep	46.5	85.7	188.5	1.295	350	33
28 days curing	**diameter (mm)**	**height (mm)**	**weight (g)**	**apparent unit weight (g/cm^3)**	**σ creep (kPa)**	**σ creep (as % UCS)**
n.1 creep	46.5	86.0	192.2	1.316	930	75
n.2 creep	46.5	85.1	189.4	1.312	700	55
n.3 creep	46.5	84.2	186.0	1.304	460	35

317 In Fig. 7 the net settlement versus time trend is reported, for the three selected curing
318 periods, respectively 1 day (A), 7 days (B) and 28 days (C). The tests have shown,
319 depending on the applied load magnitude:

320 • at 1 day of curing: a stable behavior for 2 specimens, a stable failure for 1 specimen,
321 an unstable failure for 1 specimen;

322 • at 7 days of curing: a stable behavior for 1 specimen, a stable failure for 1 specimen,
323 and unstable failure for 2 specimens;

324 • at 28 days of curing: a stable behavior for 2 specimens, an unstable failure for 1
325 specimen.

326 Fig. 8 shows some representative effects after the end of the creep test. It is possible to
327 observe how the grout can respond to a constant loading. It is necessary to remind that for
328 1 days and 7 days curing ages grout is still strengthening, even if failures occur due to
329 loading. Only for long term-curing, i.e. 28 days, it fair to state that full mechanical properties
330 of grout have been reached.

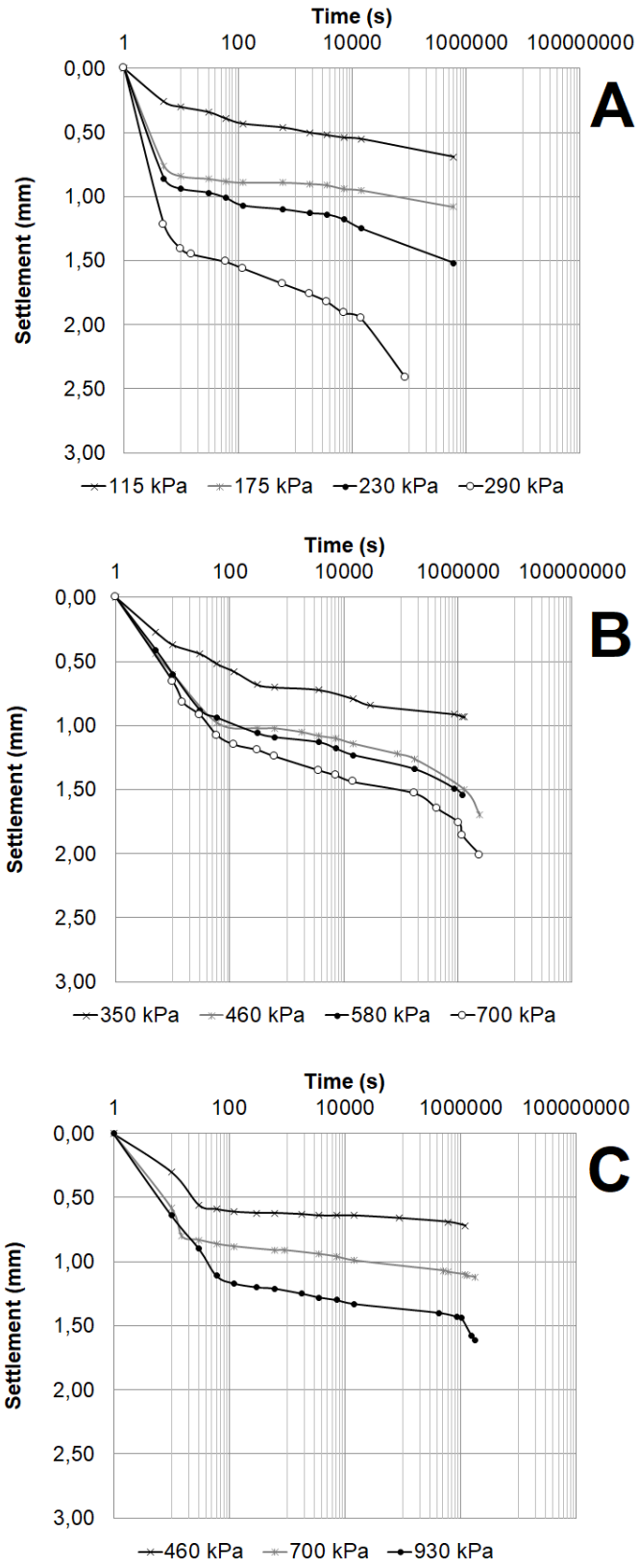

331

332 **Fig. 7 Net settlement versus time are reported, for the three selected curing periods,**

333 **respectively 1 day (graph A with 2 stable behavior, 1 stable failure, 1 unstable failure);**

7 days (graph B with 1 stable behavior, 1 stable failure, 2 unstable failure); 28 days (graph C with 2 stable behavior and 1 unstable failure).

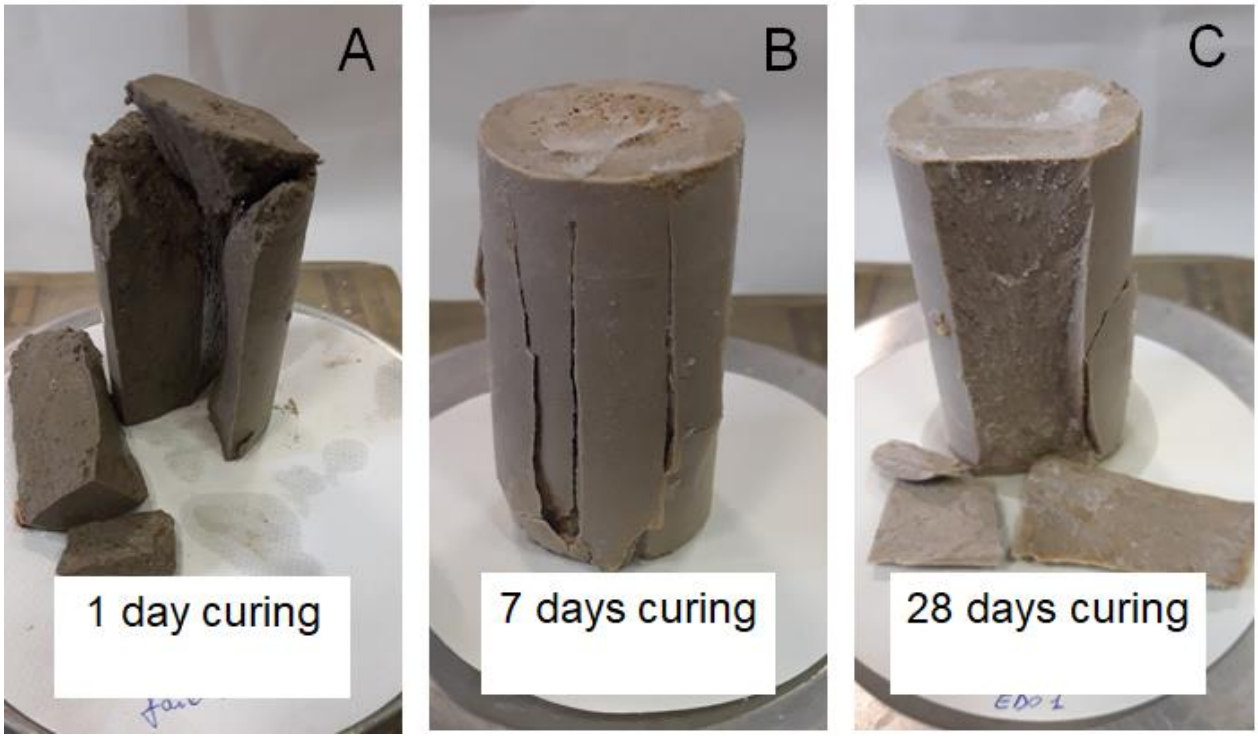

Fig. 8. Different failure modes for specimens after creep (constant load). A) de-assembled specimen, failure with conical end shape, curing 1 day; B) failure with axial symmetry for lateral expansion, 7 days curing; C) failure with conical end shape, 28 days curing.

Comments of laboratory results

The available data and the observed behavior during the standard compression test and during compression tests with constant loads (creep tests), for this mix-design, can allow to put in evidence some features:

- the mixing procedure carried directly inside the casing has determined a little increase in the unit weight referred to the test results reported in a previous campaign, thanks

to the reduction of the weak material removal from the end of the specimen during preparation;

- there is a general increase in UCS strength and in elastic moduli due to the previous point;
- all specimens have shown a post peak behavior, with wider strain softening for shorter curing ages;
- in some cases, a clear evidence of conical shaped ends at failure of the specimens has been observed, both in compression test**s** and during creep test**s**;
- long term strains do not reach an ultimate value, even when in stable loading; this happens in particular at 1 day and 7 days of curing, less for 28 days of curing. The balance between the maintained load and residual strengthening appears to be reasonably the cause for the observed trend;
- strain creep diagrams show one half of final value occur in the initial 2 minutes; there is an initial link with expected values after compression testing, then stiffness changes as a consequence of induced damage. The load in creep tests, even if less than UCS, is anyway applied instantly;
- in creep testing, for some specimens, failure has been observed as a progressive trend towards unstable crack propagation;
- no absolute and unique link between measured settlements in creep and the correspondent modulus of deformability in the compression test has been found; however satisfactory correlations exist between ΔH_{final} in stable creep zones and E_s 75% from compression tests for 1 day and 28 days of curing; in a similar way, correlation exists between $\Delta H_{primary}$ in creep and E_s 75% from compression tests for 7 days of curing;
- the deformative process results to be different for short grout curing age (1 day) respect to 7 or 28 days of curing age;

- Although temperature has an effect on creep behavior for both rocks (Li et al., 2019) and concrete (e.g. Geymayer, 1970) accelerating creep, its effects are beyond the scope of this research.

The trend of deformations over time after 7 and 28 days of curing is interesting to evaluate in order to study the effect of the creep of the two-component material on the behavior of the support system.

In particular, after 7 days of curing it is useful to refer to the curve obtained by applying an axial load equal to 33% of the failure stress (UCS) of the material (Fig. 9); this load did not cause the material to fail and a final stabilization of deformations was observed. For applied loads equal to 45% of UCS or higher (55% and 66%), on the other hand, the failure of the material was achieved after a creep phase.

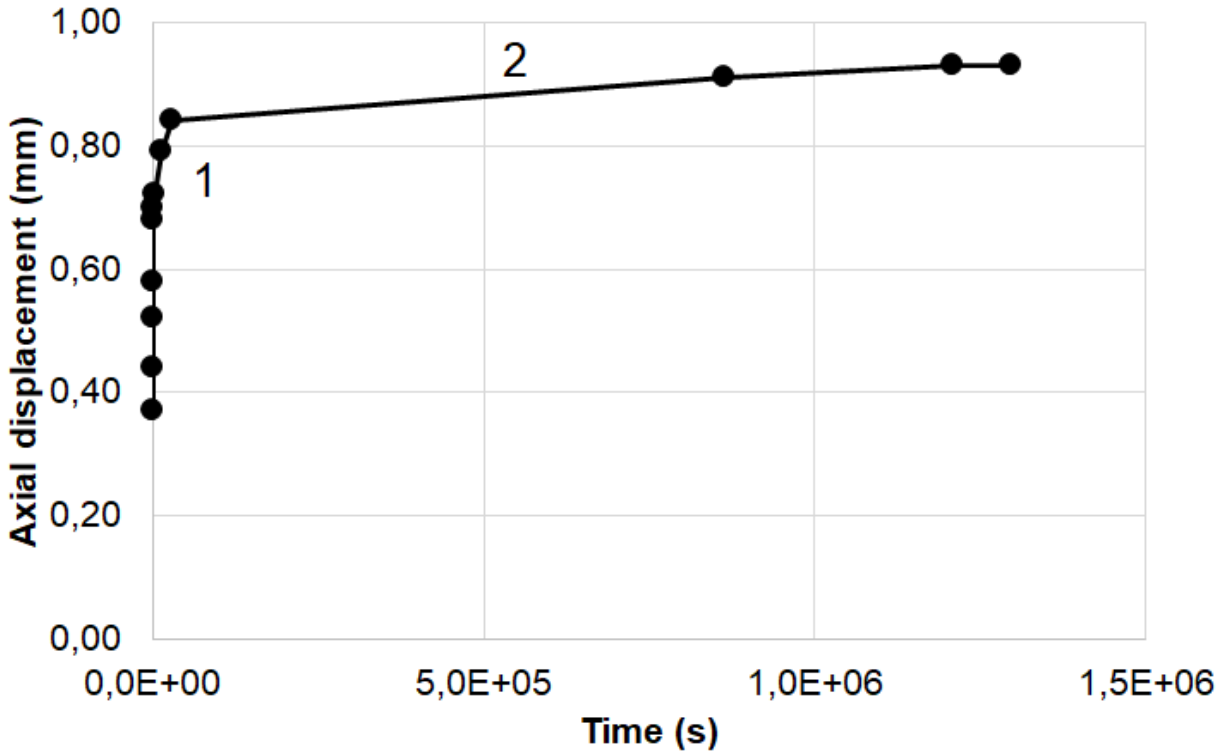

Fig. 9. Trend of deformations over time in a sample of two-component material cured for 7 days and subjected to an axial load equal to 33% of UCS. After the application of the load, there is a significant increase in displacements in the first 10 minutes,

after which the displacements grow with a markedly bi-linear trend (zones 1 and 2 in the graph) until stabilization is reached after about 14 days from loading.

From the analysis of the figure it can be seen that the immediate displacement (δ_{inst}) upon application of the load is 0.37 mm. In the first 10 minutes there is a significant increase in the displacements until reaching a double value of δ_{inst}, after which the displacements increase with a markedly bi-linear trend until stabilization is reached after about 14 days from loading: in the first linear section, the displacement changes from 2.00·δ_{inst} to 2.25·δ_{inst} after 8 hours from the application of the load; in the second linear section it reaches a displacement of 2.50·δ_{inst} after 14 days from the application of the load. The expressions that describe the trend of the displacements over time in the two linear sections are shown below:

$\delta = \left[2.00 + 0.032 \cdot \left(t - {}^{1}/_{6}\right)\right] \cdot \delta_{inst}$ (t in hours), for t ranging between 1/6 hours and 8 hours (1)

$\delta = \left[2.25 + 0.018 \cdot \left(t - {}^{1}/_{3}\right)\right] \cdot \delta_{inst}$ (t in days), for t ranging between 1/3 days and 14 days (2)

After 28 days of curing, the specimen on which a load equal to 75% of the UCS value was applied reached failure after the creep phase. While for loads equal to 35% and 55% of UCS, there was no failure of the specimen subjected to the creep test. More specifically, for the load equal to 35% of UCS we note the same bi-linear trend observed for the case referred to the 7-day curing, with a value of δ_{inst} equal to 0.30 mm. While for the load equal to 55% there is also a bi-linear trend but with the following characteristics: even now in the first 10 minutes there is a significant increase in displacements until reaching a value of 1.5·δ_{inst}; after which the displacements increase up to 1.75·δ_{inst} after 8 hours from the application of the load and in a second stretch up to the final stabilization at 14 days from the application of the load with a final displacement value equal to 2·δ_{inst}.

From a detailed analysis of the results of the creep tests, therefore, the following can be noted:

- the maximum percentage of the load with respect to UCS that would allow to avoid the failure of the specimen in the long term goes from about 40 for 1 week of curing of the material to about 70 for 4 weeks of curing of the specimen;
- the trend of deformations over time follows a bi-linear law after the first 10 minutes of loading; a first stretch is between 10 minutes and 8 hours from the application of the load, the second stretch from 8 hours to 14 days from the application of the load;
- the curing age of the specimen does not seem to alter the deformation curve over time; a certain effect on this curve is given by the applied load, evaluated as a percentage of the UCS value;
- the deformation increases according to two linear sections and the total value of the creep strain is constant and equal to one half of the immediate deformation detected on the specimen upon application of the load, regardless of the curing age of the specimen and the percentage value of the applied load;
- in the first 10 minutes from the application of the load the deformations grow rapidly until reaching 2 times the immediate deformation ($2\cdot \delta_{inst}$) for percentages of the load equal to about 35% of UCS and 1.5 times the immediate deformation ($1.5\cdot\delta_{inst}$) for percentages of the load equal to about 55% of UCS.

Immediate deformation therefore has a significant importance in understanding the phenomenon of creep because it influences the deformation levels that develop in the material over time. From the results obtained in the laboratory tests (uniaxial compression and creep), it can be seen how the initial deformation can be estimated with a good approximation by adopting the tangent elastic modulus determined in the uniaxial compression tests, associated with the stress value equal to the applied load in the creep

test. Ultimately, if the applied load is equal to 35% of UCS, the immediate deformation of the specimen ε_{inst} will be defined by the following relationship:

$$\varepsilon_{inst} = \frac{0.35 \cdot UCS}{E_{t,35\%}} \quad (3)$$

where:

UCS is the monoaxial compressive strength of the two-component material measured for a specific curing age;

$E_{t,35\%}$is the tangent modulus of elasticity measured at a stress level equal to 35% of UCS, evaluated on a specimen of two-component material with a specific curing age, subject to the uniaxial compression test.

Analysis of the effects of creep on the tunnel support system

The support system (segmental lining with the two-component material surrounding it) has been studied in detail by Oreste et al. (2021). Using the convergence-confinement method, it is possible to analyze the interaction between this support system and the tunnel wall. It is a very widespread analytical method in the geomechanical field, such as the limit equilibrium method (LEM) (Oreste, 2013), which combines the advantage of the simplicity of the approach with the precision and reliability of the results.

Some simplifying hypotheses are necessary (Osgoui and Oreste, 2007; Oreste, 2009a; 2009b; Ranjbarnia et al., 2014; 2016; Spagnoli et al., 2016):

- circular and deep tunnel;
- initial stress state of hydrostatic type (k_0 = 1);
- homogeneous and isotropic soil or rock, with linear elastic behavior.

Specific and detailed studies of the behavior of the support system can be developed by adopting three-dimensional numerical modeling (Do et al., 2014; 2015a; 2015b: Pelizza et al., 2000).

In order to evaluate the load applied on the segmental lining and the deformation conditions of the tunnel wall and of the segmental lining, it is necessary to intersect the convergence-confinement curve with the reaction line of the support system (Fig. 10) (Oreste, 2003).

The convergence-confinement curve depends on the behavior of the ground at the tunnel boundary: it relates the internal pressure applied on the tunnel wall to the radial displacement of the tunnel wall towards the center of the tunnel (Brown et al., 1983; Panet, 1995). As the internal pressure decreases, the radial displacement increases, until it reaches the maximum value when the internal pressure is zero.

The reaction line of the support system relates the pressure applied by the support system to the variation of the displacement of the tunnel wall. This displacement also corresponds to the displacement manifested by the support system on its outer edge, which comes into contact with the tunnel wall. As the movement of the tunnel wall increases, the pressure applied by the tunnel wall will increase.

There is an end equilibrium point between the tunnel and the support system which is given by the intersection between the convergence-confinement curve and the reaction line of the support system.

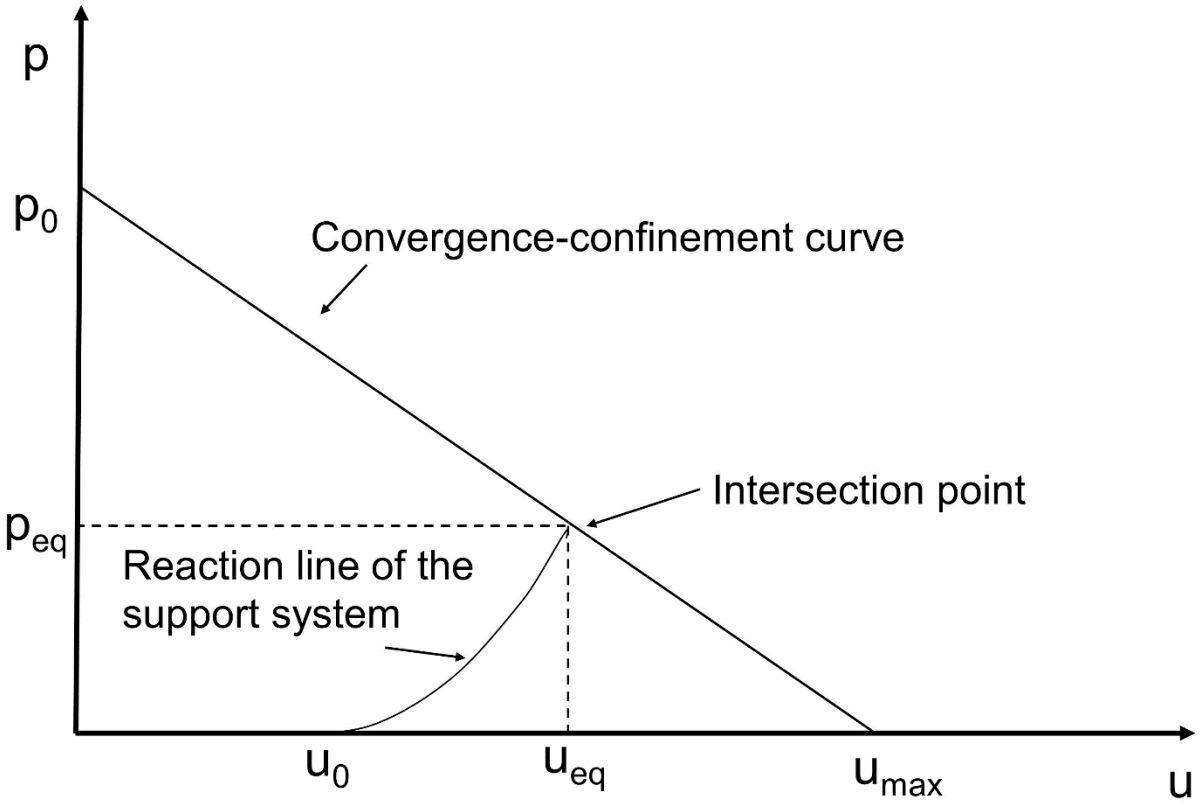

Fig. 10 The intersection between the convergence-confinement curve of the tunnel and the reaction line of the support system when this is composed of segmental lining and the two-component material around it (modified by Oreste et al., 2021). Legend: p: internal pressure applied to the tunnel wall; u: radial displacement of the tunnel wall; p_0: lithostatic stress in the soil or rock at the depth of the tunnel; u_0: displacement of the tunnel wall at the distance from the excavation face of the section where the support system is installed; $u_{max} = (1 + \nu_{gr}) \cdot p_0 \cdot R/E_{gr}$, where E_{gr} is the elastic modulus and ν_{gr} the Poisson's ratio of the ground (soil or rock) present around the tunnel; R is the tunnel radius; p_{eq} and u_{eq}: respectively the load applied on the support system and the radial displacement of the tunnel wall in the final condition of equilibrium, at the end of the process of loading the support system.

An iterative procedure was developed to correctly describe the reaction line of the support system (Oreste et al., 2021). The curvilinear shape of the reaction line is due to the fact that

the two-component material matures during the loading of the support system. There will be two specific different stiffnesses of the support system: when the segmental lining is installed, the two-component material will have a very low initial stiffness (short curing age); at the end of the support loading process (when the excavation face has advanced to a distance of about $4 \cdot R$ from the study section), the stiffness of the two-component material reaches its maximum value. This different stiffness of the support system is reflected in the inclination of the curvilinear reaction line, which initially presents a lower tangent, until reaching the maximum inclination of the tangent line near the point of intersection with the convergence-confinement curve (end of the support system loading process).

The point of intersection is given by the values p_{eq} and u_{eq} respectively the load applied on the support system and the radial displacement of the tunnel wall in the final equilibrium condition. p_{eq} and u_{eq} can be obtained from the following expressions:

$$u_{eq} = \frac{2 \cdot p_0 + u_0 \cdot \left(k_{sys,fin} + k_{sys,in}\right)}{\frac{2 \cdot E_{gr}}{(1+\nu_{gr}) \cdot R} + \left(k_{sys,fin} + k_{sys,in}\right)} \quad (4)$$

$$p_{eq} = p_0 - \frac{E_{gr}}{(1+\nu_{gr}) \cdot R} \cdot u_{eq} \quad (5)$$

where:

$k_{sys,in}$ and $k_{sys,fin}$: stiffness of the support system at the beginning and at the end of the loading process; for the evaluation of the initial stiffness, reference is made to the curing age t_0, necessary to resume the advancement of the TBM machine, which marks the start of loading of the lining; for the evaluation of the final stiffness, reference is made to the time (t_f) necessary for the excavation face to reach a distance of about $4 \cdot R$ from the studied section.

The overall stiffness of the support system is evaluated using the following equation (Oreste, 2003; Oreste et al., 2021):

$$k_{sys} = \frac{2 \cdot E_{fm} \cdot (1-\nu_{fm}) \cdot R \cdot \left[\frac{E_{fm}}{(1+\nu_{fm})} + (R-t_{fm}) \cdot k_{sl}\right]}{E_{fm} \cdot (1-2 \cdot \nu_{fm}) \cdot R^2 + (R-t_{fm})^2 \cdot \left[E_{fm} + (1-2 \cdot \nu_{fm}) \cdot (1+\nu_{fm}) \cdot k_{sl} \cdot t_{fm} \cdot \left(1 + \frac{R}{(R-t_{fm})}\right)\right]} - \frac{E_{fm}}{(1+\nu_{fm}) \cdot R} \quad (6)$$

where:

$$k_{sl} = \frac{E_{sl}}{(1+\nu_{sl})} \cdot \frac{(R-t_{fm})^2 - (R-t_{fm}-t_{sl})^2}{(1-2 \cdot \nu_{sl}) \cdot (R-t_{fm})^2 + (R-t_{fm}-t_{sl})^2} \cdot \frac{1}{(R-t_{fm})}$$

k_{sl} is the radial stiffness of the segmental lining;

E_{fm} and ν_{fm} are respectively the elastic modulus and the Poisson's ratio of the filling material; E_{fm} varies over time with increasing curing age;

E_{sl} and ν_{sl} are respectively the elastic modulus and the Poisson's ratio of the segmental lining;

t_{fm} and t_{sl} are respectively the thickness of the filling material and of the segmental lining.

To determine the k_{sys} values it is necessary to evaluate the elastic modulus of the filling material E_{fm}. Imagining a progressive loading over time with a regular advancement of the excavation face, the deformation process that develops in the filling material is the one that refers to the first minutes of the creep tests.

Therefore, for the evaluation of the $k_{sys,in}$ reference must be made to the initial tangent elastic modulus ($E_{fm} = E_{t,0\%}$ of the filling material). To determine $k_{sys,fin}$ a value of the elastic modulus of the filling material must be adopted which depends on the stress level reached inside it in the final equilibrium condition:

$$E_{fm} \cong \frac{E_{t,\alpha}}{\omega} \quad (7)$$

where:

535 $E_{t,\alpha}$ is the tangent elastic modulus of the filling material associated with a percentage load
536 level α referred to UCS;

537 ω is a correction coefficient that takes into account the deformation increase that occurs in
538 the first 10 minutes of load in the creep test; it depends on the percentage α of the stress
539 level acting in the filling material with respect to the UCS strength, i.e. $\omega = 2.875 - 2.5 \cdot \alpha$.

540 Since the stress state induced in the filling material depends on the still unknown value of
541 p_{eq}, also in this case the value of E_{fm} must be adapted as a function of p_{eq} and u_{eq}, which
542 is obtained from the intersection of the two curves. Another iterative procedure is therefore
543 necessary.

544 The value of the maximum principal stress in the filling material can be obtained from the
545 following expression (Oreste et al., 2021):

546 $$\sigma_{1,max,fm} \cong \frac{u_{eq} \cdot \frac{E_{fm}(t_f)+E_{fm}(t_0)}{2 \cdot R} + \left(\nu_{fm}+\nu_{fm}^2\right) \cdot p_{eq}}{\left(1-\nu_{fm}^2\right)} \quad (8)$$

547 where: $\sigma_{1,max,fm}$ is the maximum (circumferential) principal stress in the filling material.

548 The value α will be adapted until the values of p_{eq}, u_{eq}, $\sigma_{1,max,fm}$ and UCS are compatible
549 with each other. At that point, the reaction line of the support system can be correctly placed
550 in the graph and p_{eq} and u_{eq} evaluated.

551 Once the final configuration of the support system has been reached, it will be possible to
552 represent the effect of the creep on the bilinear tract of Fig. 9. On the basis of the
553 experimentation carried out and what was deduced in the previous paragraph, the overall
554 deformation increase due to the creep phenomenon can be estimated as half of the
555 immediate deformation, regardless of the curing age of the specimen and the value of the
556 applied load. It is therefore possible to derive the increase in deformation due to the creep
557 in the filling material from the following expression:

$$\varepsilon_{creep} = 0.5 \cdot \frac{\sigma_{1,max,fm}}{E_{t,\alpha}} \quad (9)$$

Since this deformation ε_{creep} is a circumferential deformation at the extrados of the filling material ring, it is possible to derive from it the increase in displacement Δu of the tunnel wall:

$$\Delta u = \varepsilon_{creep} \cdot R \quad (10)$$

Thanks to the knowledge of Δu it will be possible to represent the effect of the creep of the filling material on the graph of the convergence-confinement curve and evaluate the final displacement of the tunnel wall (Fig. 11).

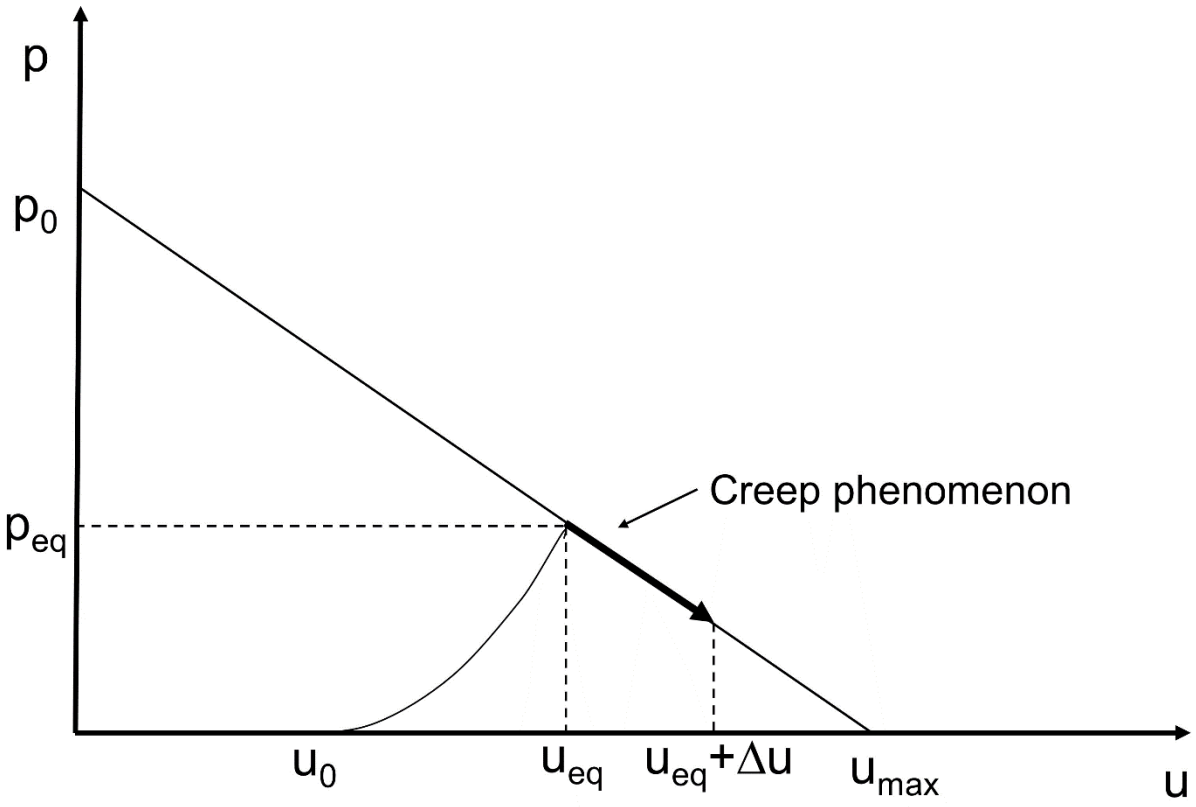

Fig. 11. Representation of the creep phenomenon in the filling material once the final equilibrium point is reached at the end of the process of placing the support system in charge. Legend: Δu: increase in the radial displacement of the tunnel wall due to the creep of the filling material.

571 The creep phenomenon therefore produces an increase in the displacement of the tunnel
572 wall, as well as a stress discharge of the segmental lining. Both results are fundamental for
573 tunnel design. The increase in the displacement of the tunnel wall is useful for evaluating
574 the subsidence of the soil surface in the long term. The stress relief of the segmental lining
575 allows to obtain the correct value of the safety factor of the support system in the long term.
576 Furthermore, the increase in the displacement of the tunnel wall as a result of the creep can
577 lead to values exceeding the maximum acceptable limits, such as to indicate an incorrect
578 functioning of the tunnel-support system. The final control of this displacement in the tunnel
579 design stage, therefore, is essential to avoid excessive values which could lead to high risks
580 of instability of the tunnel.

581 **Example of support system design considering the filling material creep phenomenon**

582 In defining the thickness of the filling material and also the thickness of the segmental lining,
583 it is necessary to consider the evolution over time of the mechanical characteristics of the
584 filling material (following its curing) and the creep phenomenon. In fact, the curing over time
585 and the creep phenomenon markedly characterize the two-component material and
586 influence the loading of the support system. The final load acting on the segmental lining,
587 therefore, depends on the thickness of the filling material and on the methods of loading the
588 support system. Oreste et al. (2021) have already demonstrated how the thickness of the
589 filling material, the downtime of the TBM machine after the construction of the support
590 system, the average speed of advancement of the TBM after the stop of the TBM are all
591 elements that influence the stress state in the filling material and the load acting on the
592 support system.

593 More specifically, the case of a tunnel with a length of 5 km and a diameter of 9.4 m,
594 excavated at a depth of about 70 m (p_0 = 1.12 MPa) in Northern Italy by a TBM machine
595 (EPB type) in a weakly cohesive soil having an elastic modulus E_{gr} of 150 MPa and a

Poisson's ratio v_{gr} of 0.3 was analyzed in detail. The thickness adopted for the segmental lining (t_{sl}) was 0.35 m, the thickness of the filling material (t_{fm}) was 0.15 m. For the segmental lining concrete, an elastic modulus E_{sl} of 30,000 MPa and a Poisson's ratio v_{sl} of 0.15 were assumed.

Considering a still stand for the construction of a new lining ring of 1 hour at a distance of 2.5 m from the excavation face and an average advancement speed of the TBM v of 0.35 m/h, the reaction line of the reported support system is shown in Figure 12 (modified after Oreste et al., 2021).

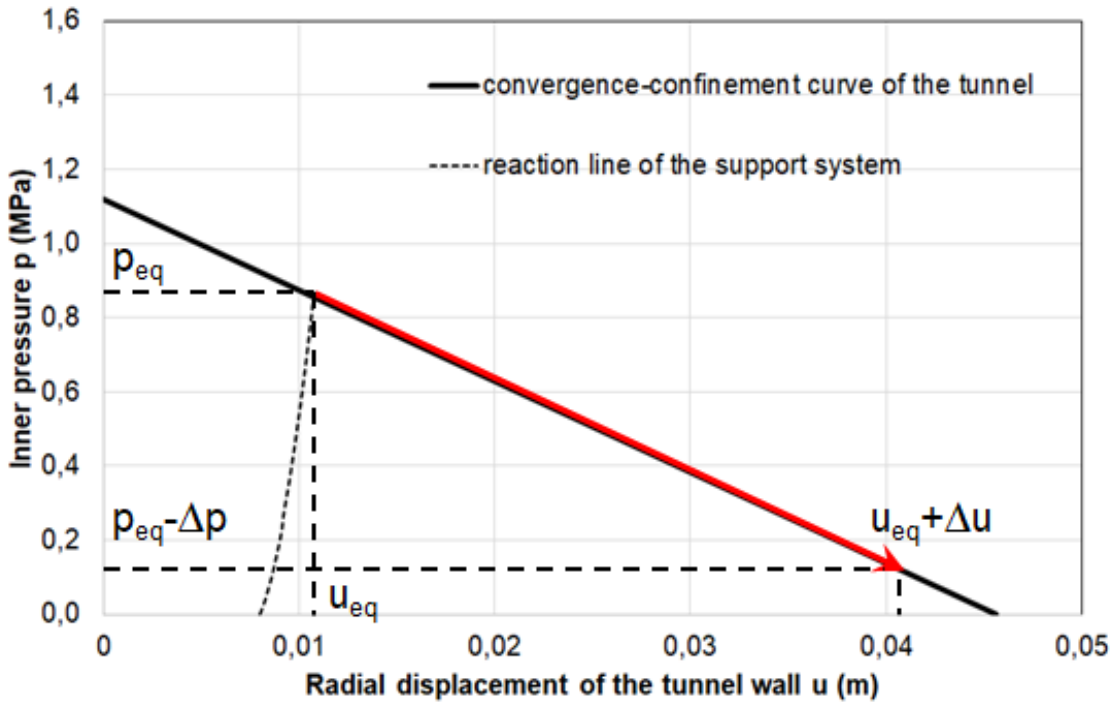

Fig. 12. Convergence-confinement curve of the tunnel and reaction line of the support system in the examined case: tunnel with a diameter of 9.4 m at a depth of 70 m excavated in a weakly cohesive soil with an elastic modulus E_{gr} of 150 MPa. The support system consists of a 0.35 m thick segmental lining and a 0.15 m thick filling material ring. The red line represents the modification of the equilibrium point on the

convergence-confinement curve following the creep phenomenon in the filling material.

The pressure p_{eq} associated with the intersection point is 0.86 MPa and represents the load acting on the support system at the end of the loading process, when the excavation face reaches a distance of about $4 \cdot R$ from the study section of the support system. The displacement u_{eq} is 10.7 mm: it is the final displacement of the tunnel wall at the end of the loading process.

Using eq. 8 it is possible to determine $\sigma_{1,max,fm}$, the maximum (circumferential) principal stress in the filling material at the end of the loading of the support system; a value of 0.92 MPa is obtained, which constitutes 31.6% of the strength of the material after about 48 h, the average time necessary to reach the distance of $4 \cdot R$ from the investigated section.

From the experimental study developed and presented in the previous paragraphs, it was possible to verify how the long-term strength of the two-component material is only a percentage η of the UCS. In particular, the value of η depends on the days of curing of the material:

$$\eta \cong 0.3 + 0.0143 \cdot t_c \quad (11)$$

Where:

t_c is the curing age in days**.**

After two days of curing (48 h), therefore, η worth about 32.9%. This means, therefore, that a maximum stress of 0.92 MPa (31.6% of the compressive strength UCS) is bearable by the two-component material even in the long term without reaching failure. By maintaining its integrity, the two-component material is able to effectively perform the task of transferring

632 the radial loads to the segmental lining and allowing the support system to be waterproofed,
633 preventing water from infiltrating inside the tunnel.

634 As for the deformation increase of the tunnel wall, the value of Δu can be determined on the
635 basis of equations 9 and 10 and considering that the stress $\sigma_{1,max,fm}$ inside the two-
636 component material tends to decrease progressively during the creep phase: it is therefore
637 necessary to adopt the average value that this stress assumes in this specific phase.
638 Therefore, assuming a tangent elastic modulus E_t at two days of curing equal to 40 MPa,
639 we obtain a ε_{creep} value of 0.0067 and an increase in the radial displacement of the tunnel
640 wall of about 31 mm. This increase in the deformations of the tunnel wall has the effect of
641 reducing the load applied on the segmental lining from the initial value of 0.86 MPa to the
642 final value (at the end of the creep phase) of 0.11 MPa. A consistent reduction of the acting
643 loads and of the stress state induced in the concrete which is often found when detailed
644 measures for monitoring the behavior of the segmental lining are available long times after
645 its installation.

646 **Conclusions**

647 The filling material inserted in the gap between the segmental lining and the tunnel wall has
648 several important roles aimed at ensuring the effectiveness of the support system of a tunnel
649 excavated with a TBM machine. Nowadays a **bi**-component filling material is widely used,
650 which has particular characteristics: a curing phase during which the mechanical parameters
651 evolve rapidly; a creep behavior with secondary deformations that develop over time when
652 the material is subjected to a stress load. These features make the interaction between the
653 support system and the tunnel complex, given that the filling material is loaded progressively
654 over time, starting from its installation into the gap between the segmental lining and the
655 tunnel wall. The creep phase generally comes into play at the end of the support system

loading phase and has as a consequence the reduction of the loads transmitted to the segmental lining and the increase in deformations of the tunnel wall.

The creep phenomenon has been studied for many other materials in the field of geotechnics and geomechanics. Many models have been developed and are known in the scientific literature to represent the behavior of such materials. Although the two effects mentioned above and induced by the creep of the filling material on the extrados of the segmental lining are very important, no studies on this topic are available in the literature.

In particular, the increase in the radial displacement of the tunnel wall due to the phenomenon of creep in the filling material can induce high subsidence on the soil surface and can lead to conditions that are not compatible with the stability of the tunnel (exceeding the maximum permissible values of the convergence tunnel).

In this work the results of an extensive laboratory experimentation on the creep behavior, developed for different curing ages of the specimens and different load entities in relation to the UCS of the material, are reported. It was possible to identify which is the maximum compression stress where no failure of the material under a continuous load over time is observed. In addition, it was possible to derive the recurring trend of deformations over time (creep trend) by varying the curing ages and the stress state applied to the specimens.

The information obtained from the experimentation was then used to understand the effects of the creep phase of the two-component material on the interaction between the support system and the tunnel. In particular, it was possible to evaluate the decrease in the radial load applied to the support system (and, therefore, to the segmental lining) and the increase in the deformations of the tunnel wall. Finally, the application of the above considerations to a real case of a tunnel excavated in Northern Italy in a weakly cohesive ground has allowed to understand how the creep of the two-component material has non-negligible effects on

680 the final stress state induced in the segmental lining and on radial displacements of the
681 tunnel wall.

682 **Acknowledgment**

683 The authors wish to thank Master Builders Solutions by MBCC Group for the permission
684 granted to publish the results and to the reviewers' comments which increased the quality
685 of the manuscript.

686 **Conflict of interests**

687 Authors declare they have no conflict of interest.

688 **References**

689 Arnau, O., Molins, C., Blom, C.B.M., Walraven, J. (2011). Longitudinal time-dependent
690 response of segmental tunnel linings. Tunnelling and Underground Space Technology
691 28(1):98, *10.1016/j.tust.2011.10.002*.

692 Barla, G. (2011). Contributions to the understanding of time dependent behaviour in deep
693 tunnels. Geomech Tunnelling; 4: 255-264.

694 Brown E.T., Bray J.W., Ladanyi B., Hoek E. (1983). Ground response curves for rock
695 tunnels. Journal of Geotechnical Engineering,109, 1, 15-39
696 https://doi.org/10.1061/(ASCE)0733-9410(1983)109:1(15)

697 Cardu, M. and Oreste, P. (2012). Technical-operational comparison between trench-cutters
698 and clam excavators for concrete diaphragm construction in underground works at shallow
699 depths. Int. J. Min. Reclamat. Environ., 26, 3, 217–232.

700 Di Giulio, A.. Bavasso, I., Di Felice, M.. and Sebastiani, D. (2020). A preliminary study of the
701 parameters influencing the performance of two-component backfill grout. Gallerie e Grandi
702 Opere Sotterranee. 133. 11-17.

703 Do N.A., Dias D., Oreste P. (2014). Three-dimensional numerical simulation of mechanized
704 twin stacked tunnels in soft ground, Journal of Zhejiang University: Science A, 15(11):896–
705 913.
706 Do N.A., Dias D., Oreste P., Djeran-Maigre I. (2015a). 2D numerical investigation of
707 segmental tunnel lining under seismic loading. Soil Dynamics and Earthquake Engineering
708 72 (2015): 66-76.
709 Do N.A., Dias D., Oreste P. (2015b). 3D numerical investigation on the interaction between
710 mechanized twin tunnels in soft ground. Environmental Earth Sciences, 73(5):2101–2113.
711 Dusseault. M.B. Fordham. C.J. 1993. Time-dependent behavior of rocks. In Hudson JA. ed.
712 Comprehensive Rock Engineering. Pergamon Press: 119–149.
713 Farmer I.W. and Gilbert M.J. (1981). Time dependent strength reduction of rock salt. Proc.
714 1st Conf. on Mechanical Behaviour of Rock Salt, Pennsylvania State Univ.
715 Flores, A.Q. (2015). Physical and mechanical behavior of a two component cement-based
716 grout for mechanized tunneling application. MSc Thesis. Universidade Federal do Rio de
717 Janeiro. Brazil.
718 Geymayer, H.G. (1970). The effect of temperature on creep of concrete: a literature review.
719 U.S. Army Engineer Waterways Experiment Station Corps of Engineers, Vicksburg,
720 Mississippi.
721 Goodman, R. (1980). Introduction to Rock Mechanics. New York: Wiley.
722 Griggs, D. (1939). Creep of rocks. The Journal of Geology, 47, 3, 225-251.
723 Hardy H.R., Kim R.Y., Stefanko R. and Wang Y.J. (1969). Creep and microseismic activity
724 in geologic materials. Proc. 13th US Rock Mech. Symp., Berkeley, 377-413.
725 Hirata, T. (1989). Study on behavior of cohesive soil in type shield tunneling work and on
726 construction technique. Doctoral Thesis. Kyoto University. Japan.
727 Huber, H.G. (1991). Untersuchung zum Verformungsverhalten von jungem Spritzbeton im
728 Tunnelbau. Master Thesis. University of Innsbruck. Austria.

729 Jaeger, J.C.. Cook. N.G.W. (1979). Fundamentals of Rock Mechanics. London: Chapman
730 and Hall.
731 Kuwajima, F.M. Early age properties of the shotcrete. In Shotcrete for Underground VIII.
732 Celestino. T.B. and Parker. H.W.. eds.. Conference Eighth International Conference. São
733 Paulo. Brazil, April 11-15. 1999. American Society of Civil Engineers. Reston. VA.
734 Lama R.D. and Vutukuri V.S. (1978). Handbook on mechanical properties of rock. Testing
735 techniques and results. Vol. III, Trans Tech Publ.
736 Li., J., Sun. G., Zou, H., Zhou, Z., Fan, X. (2019). Influence of temperature and load on creep
737 characteristics of soft rock similar materials. IOP Conf. Series: Earth and Environmental
738 Science 384, 012229, doi:10.1088/1755-1315/384/1/012229.
739 Melbye, T. (1994). Sprayed Concrete for Rock Support. Switzerland: MBT Underground
740 Construction Group.
741 Ochmański, M.. Modoni, G. and Bzówka, J. (2018). Automated numerical modelling for the
742 control of EPB technology. Tunnelling and Underground Space Technology 75. 117–128.
743 *https://doi.org/10.1016/j.tust.2018.02.006*.
744 Ochmański, M., Modoni. G. and Spagnoli, G. (2021). Influence of the annulus grout on the
745 soil-lining interaction for EBP tunneling. Geotechnical Aspects of Underground Construction
746 in Soft Ground: Proceedings of the Tenth International Symposium on Geotechnical Aspects
747 of Underground Construction in Soft Ground, IS-Cambridge 2022, Cambridge, United
748 Kingdom, 27-29 June 2022, 350-356, DOI: *10.1201/9780429321559-45*
749 Oggeri, C.. Oreste, P.. and Spagnoli, G. (2021). The influence of the two-component grout
750 on the behaviour of a segmental lining in tunnelling. Tunnelling and Underground Space
751 Technology. 109. 103750. *https://doi.org/10.1016/j.tust.2020.103750*.
752 Oh, J.Y. and Ziegler, M. (2014). Investigation on influence of tail void grouting on the surface
753 settlements during shield tunneling using a stress-pore pressure coupled analysis. KSCE
754 Journal of Civil Engineering. 18(3). 803-811. DOI: *10.1007/s12205-014-1383-8*.

Oreste P. (2003). Analysis of structural interaction in tunnels using the covergence–confinement approach, Tunnelling and Underground Space Technology, 18, 4, 347-363.

Oreste, P. (2007). A numerical approach to the hyperstatic reaction method for the dimensioning of tunnel supports. Tunnelling and Underground Space Technology 22(2):185–205. https://doi.org/10.1016/j.tust.2006.05.002.

Oreste P (2009a). The convergence-confinement method: roles and limits in modern geomechanical tunnel design. American Journal of Applied Sciences 6(4):757-771.

Oreste P (2009b). Face stabilisation of shallow tunnels using fibreglass dowels. Proceedings of the Institution of Civil Engineers-Geotechnical Engineering, 162(2):95-109.

Oreste P. (2013). Face stabilization of deep tunnels using longitudinal fibreglass dowels. International Journal of Rock Mechanics and Mining Sciences, 58:127-140.

Oreste P (2015). Analysis of the interaction between the lining of a TBM tunnel and the ground using the convergence-confinement method. American Journal of Applied Sciences 12(4):276-283. DOI: 10.3844/ajassp.2015.276.283.

Oreste P., Spagnoli G., Ceravolo LA (2019) A numerical model to assess the creep of shotcrete linings. Proceedings of the Institution of Civil Engineers – Geotechnical Engineering. 172. 4. 344-354. *https://doi.org/10.1680/jgeen.18.00089*.

Oreste, P., Spagnoli, G., Luna Ramos, C.A. (2020). Evaluation of the safety factors of shotcrete linings during the creep stage. Proceedings of the Institution of Civil Engineers – Geotechnical Engineering. 173. 3. 274-282. *https://doi.org/10.1680/jgeen.19.00104*

Oreste, P., Sebastiani, D., Spagnoli, G., de Lillis, A. (2021) Analysis of the behavior of the two-component grout around a tunnel segmental lining on the basis of experimental results and analytical approaches. Transportation Geotechnics, 29, 100570, *https://doi.org/10.1016/j.trgeo.2021.100570*

779 Orumchi, H. and Mojallal, M. (2017). Shear Strength Design of a Mechanized Tunneling
780 Grout Mix: Case Study of the Tehran Subway Line 6 Project. Transp. Infrastruct. Geotech.
781 4, 18–36. *https://doi.org/10.1007/s40515-017-0037-7*
782 Osgoui, R., and Oreste, P. (2007). Convergence-control approach for rock tunnels
783 reinforced by grouted bolts, using the homogenization concept. Geotechnical and
784 Geological Engineering 25(4):431-440, DOI: *10.1007/s10706-007-9120-0*.
785 Panet, M. (1995). Calcul des Tunnels par la Mdthode de ConvergenceConfinement. Paris:
786 Press de l'Ecole Nationale des Ponts et Chausses.
787 Pelizza S., Oreste P., Peila D., Oggeri C. (2000). Stability analysis of a large cavern in Italy
788 for quarrying exploitation of a pink marble. Tunnelling and Underground Space Technology,
789 15(4):421–435.
790 Price A.M. and Farmer I.W. (1981). The Hvorslev surface in rock deformation. Int. Journ. Of
791 Rock Mech. And Min.Sci., 18, 229-34.
792 Ranjbarnia M., Fahimifar A., Oreste P. (2014). A simplified model to study the behavior of
793 pre-tensioned fully grouted bolts around tunnels and to analyze the more important
794 influencing parameters. Journal of Mining Science 50(3):533-548
795 Ranjbarnia, M., Fahimifar, A., Oreste, P. (2016). Practical method for the design of
796 pretensioned fully grouted rockbolts in tunnels. International Journal of Geomechanics,
797 16(1), 04015012
798 Rahmati, S., Chakeri. H., Sharghi. M., Dias, D. 2021. Experimental study of the mechanical
799 properties of two-component backfilling grout. Proceedings of the Institution of Civil
800 Engineers - Ground Improvement. *https://doi.org/10.1680/jgrim.20.00037*.
801 Rokahr, R.B. Lux, K.H. (1987). Einfluss des rheologischen Verhaltens des Spritzbetons auf
802 den Ausbauwiderstand. Felsbau. 5:11-18.

Shah, R.. Lavasan, A.A. , Peila. D., Todaro. C., Luciani. A. and Schanz, T. (2018). Numerical study on backfilling the tail void using a two-component grout. J. Mater. Civ. Eng.. 30(3): 04018003.

Sharghi, M. , Chakeri, H. , Afshin. H. , and Ozcelik, Y. 2018. An experimental study of the performance of two-component backfilling grout used behind the aegmental lining of a Tunnel-Boring Machine. Journal of Testing and Evaluation. 46. 5. 2083–2099. *https://doi.org/10.1520/JTE20160617*.

Spagnoli G. Oreste P. Lo Bianco L. (2016). New equations for estimating radial loads on deep shaft linings in weak rocks. International Journal of Geomechanics 16(6): 06016006. DOI: *10.1061/(ASCE)GM.1943-5622.0000657*.

Spagnoli G., Miedema S.A., Herrmann, C., Rongau J., Weixler, L. Denegre J. (2016) Preliminary Design of a Trench Cutter System for Deep-Sea Mining Applications Under Hyperbaric Conditions. IEEE Journal of Oceanic Engineering 41, 4, 930 – 943, *10.1109/JOE.2015.2497884*.

Thewes, M. and Budach, C. (2009). Grouting of the annular gap in shield tunnelling-An important factor for minimisation of settlements and production performance. Proceedings of the ITA-AITES World Tunnel Congress 2009 “Safe Tunnelling for the City and Environment”. pp. 1–9.

Thomas, A. (2009). Sprayed concrete lined tunnels. Oxon: Taylor and Francis.

Todaro. C., Peila. L., Luciani. A., Carigi. A.. Martinelli, D. and Boscaro, A. (2019). Two component backfilling in shield tunneling: laboratory procedure and results of a test campaign. In Proceedings of the WTC 2019 ITA-AITES World Tunnel Congress (WTC 2019). May 3-9. 2019. Naples. Italy. Peila. D.. Viggiani. G. and Celestino. T. (eds). CRC Press. Boca Raton.

827 Van der Schyff J.J. (2017). Quantifying the creep behaviour of polyester resin and grout.
828 Proceedings of the 17th Coal Operators' Conference, Mining Engineering, University of
829 Wollongong.
830 Yin, J. (1996). Untersuchungen zum zeitabhängigen Tragverhalten von tiefliegenden
831 Hohlraumen im Fels mit Spritzbeton. PhD Thesis. Clausthal University of Technology.
832 Germany.
833 Yu, C.W. 1998. Creep characteristics of soft rock and modelling of creep in tunnel:
834 determination of creep characteristics of soft rock and development of non-linear creep
835 analysis code for squeezing tunnel problem. PhD Thesis. University of Bradford. UK.

FIGURE CAPTION

Fig. 1 Section of EPB-TBM with some main aspects highlighted

Fig. 2: Two examples of creep with a staged loading on evaporitic rocks. Specimen a) is entirely made of salt, with microcrystals from millimetric to centimetric size (see figure on the right); after an initial stable load at 14.1 MPa, failure is reached with a step at 18.8 MPa. Specimen b) is a fine-grained salt including elements of marl; after an initial load at 29.9 MPa, failure is reached with a step at 34.2 MPa.

Fig. 3 Left: Twin cells adapted in the oedometer frame, where specimens are kept submerged during constant load application and vertical settlement of the base is continuously measured. Right: detail of a specimen inside a testing cell.

Fig. 4 Example of standard specimens prepared and obtained for UCS and creep testing. The grain size of the cured grout specimens appears regular and homogeneous, without veins or lenses of different consistency.

Fig. 5. Examples of vertical stress – vertical strain curves for grout specimens at different curing age (at 24 hours, 7 days and 28 days from curing beginning, respectively), during a uniaxial compressive test. Along the vertical axis applied stress σ in MPa is reported, along horizontal axis induced vertical strain in ε (ratio of the vertical displacement on the sample height) is reported. Strain softening after the stress peak is more evident for short age curing specimens.

Fig. 6. Different failure modes for specimens after unconfined compression testing. The formation of conical shaped bodies is clearly visible at left and in the middle. On the right, the radial expansion has prevailed with symmetrical formation of vertical slabs.

Fig. 7 Net settlement versus time are reported, for the three selected curing periods, respectively 1 day (graph A with 2 stable behavior, 1 stable failure, 1 unstable failure); 7 days (graph B with 1 stable behavior, 1 stable failure, 2 unstable failure); 28 days (graph C with 2 stable behavior and 1 unstable failure).

Fig. 8. Different failure modes for specimens after creep (constant load). A) de-assembled specimen, failure with conical end shape, curing 1 day; B) failure with axial symmetry for lateral expansion, 7 days curing; C) failure with conical end shape, 28 days curing.

Fig. 9. Trend of deformations over time in a sample of two-component material cured for 7 days and subjected to an axial load equal to 33% of UCS. After the application of the load, there is a significant increase in displacements in the first 10 minutes, after which the displacements grow with a markedly bi-linear trend (zones 1 and 2 in the graph) until stabilization is reached after about 14 days from loading.

Fig. 10 The intersection between the convergence-confinement curve of the tunnel and the reaction line of the support system when this is composed of segmental lining and the two-component material around it (modified by Oreste et al., 2021). Legend: p: internal pressure applied to the tunnel wall; u: radial displacement of the tunnel wall; p_0: lithostatic stress in the soil or rock at the depth of the tunnel; u_0: displacement of the tunnel wall at the distance from the excavation face of the section where the support system is installed; $u_{max} = (1 + \nu_{gr}) \cdot p_0 \cdot R/E_{gr}$, where E_{gr} is the elastic modulus and ν_{gr} the Poisson's ratio of the ground (soil or rock) present around the tunnel; R is the tunnel radius; p_{eq} and u_{eq}: respectively the load applied on the support system and the radial displacement of the tunnel wall in the final condition of equilibrium, at the end of the process of loading the support system.

Fig. 11. Representation of the creep phenomenon in the filling material once the final equilibrium point is reached at the end of the process of placing the support system in charge. Legend: Δu: increase in the radial displacement of the tunnel wall due to the creep of the filling material.

Fig. 12. Convergence-confinement curve of the tunnel and reaction line of the support system in the examined case: tunnel with a diameter of 9.4 m at a depth of 70 m excavated in a weakly cohesive soil with an elastic modulus E_{gr} of 150 MPa. The support system consists of a 0.35 m thick segmental lining and a 0.15 m thick filling material ring. The red line represents the modification of the equilibrium point on the convergence-confinement curve following the creep phenomenon in the filling material.

Creep behaviour of two-component grout and interaction with segmental lining in tunnelling

Claudio Oggeri[1], Pierpaolo Oreste[1], Giovanni Spagnoli[2]*

[1] Department of Environment, Land and Infrastructure Engineering, Politecnico di Torino, Corso Duca Degli Abruzzi 24, 10129 Torino, Italy

[2] MBCC Group, Dr-Albert-Frank-Strasse 32, 83308 Trostberg, Germany, Tel: +49 8621 86-3702, *giovanni.spagnoli@mbcc-group.com* ORCID: 0000-0002-1866-4345 (CORRESPONDING AUTHOR)

Abstract

The complexity of the two-component grout behavior significantly affects the interaction between the support system and the tunnel. The loading of the filling material (and also of the segmental lining) takes place during the curing phase. At the end of it a creep phase develops which shows secondary deformations over time which result in a relaxation of the segmental lining and an increase in the deformation of the tunnel wall. In this work, a laboratory experiment campaign allowed to study the two-component material in detail during the creep phase. The typical trend of deformations over time, obtained for different stress load values and material curing age, was identified. The maximum stress was also evaluated which still allows to avoid the failure of the material over time, when a persistent state of stress is applied. The information obtained from the experimentation allowed to provide considerations on the support system-tunnel interaction, using the convergence-confinement method. The approach followed was then applied to a real case of a tunnel excavated in Northern Italy, for which it was possible to estimate the decrease in the load applied to the support system and the increase in deformations of the tunnel wall due to the creep phenomenon of the two-component material.

Key words: two-component grout; curing age; Tunnel Boring Machine (TBM); convergence-confinement method (CCM); creep-behaviour.

Abbreviations and nomenclature

E_{fm} Elastic modulus of the filling material

E_{gr} Elastic modulus of the ground

E_s Secant elastic modulus

E_{sl} Elastic modulus of the segmental lining (concrete)

E_t Tangent elastic modulus

$E_{t,\alpha}$ Tangent elastic modulus of the filling material associated with a percentage load level α referred to the Unconfined Compressive Strength (UCS)

$E_{t,35\%}$ Tangent modulus of elasticity measured at a stress level equal to 35% of UCS

$k_{sys,fin}$ Stiffness of the support system at the end of the loading process

k_{sys} Stiffness of the support system

$k_{sys,in}$ Stiffness of the support system at the beginning of the loading process

k_{sl} Radial stiffness of the segmental lining

k_0 Coefficient of earth pressure at rest

p Pressure inside the tunnel acting on the walls

p_{eq} Final entity of the loads acting on the support system

p_0 Hydrostatic initial stress state (undisturbed)

R Tunnel radius

t_{fm} Thickness of the filling material

t_{sl} Thickness of the segmental lining

UCS Unconfined compressive strength

u_{eq} Final entity of the tunnel wall displacement

u_0 Displacement of the tunnel wall when the support system is installed

u_{max} Maximum displacement of the tunnel wall in the absence of supports

ν_{fm} Poisson's ratio of the filling material

ν_{gr} Poisson's ratio of the soil or rock present around the tunnel

ν_{sl} Poisson's ratio of the concrete constituting the segmental lining

α Percentage of the stress level acting in the filling material with respect to the UCS strength

δ_{inst} Immediate displacement in the filling material

ε strain (ratio of the the displacement on the reference height)

ε_{creep} creep strain of the filling material

ε_{inst} Immediate deformation of the filling material

η Long-term strength of the two-component material as a percentage of the UCS

ω Correction coefficient taking into account the deformation increase that occurs in the first 10 minutes of load during a creep test

σ Applied or induced stress

Δu	Increase in the radial displacement of the tunnel wall due to the creep phenomenon of the filling material

Introduction

The backfilling (or tail void grouting) is the system used during the excavation of a tunnel by means of a TBM (Tunnel Boring machine) to fill the void created during the advancement of the machine between the support structure and the rock wall. As a matter of fact, when tunneling is carried out using a shield machine and a segmental lining, there is a gap caused by the overcut due to the slightly larger diameter of the shield machine than the lining (Sharghi et al., 2018) and to the thickness of the shield and the space occupied by the brushed, which close the void lining-shield (see Fig. 1). This gap is needed in order for the TBM to curve left/right (planimetric curves) or up/down (altimetric curves).

The instantaneous filling of the annulus that is created behind the segment lining at the end of the TBM tail during its advancement is a very important operation. The objective is to minimize the surface settlements induced by the passage of the TBM, to assure that the tunnel convergence is within the allowable limit, to ensure the homogeneous transmission of stresses between the soil/rock mass and the lining, to avoid misalignments of the linings and to provide impermeabilization of the tunnel (Thewes and Budach, 2009; Di Giulio et al., 2020; Oggeri et al., 2021). Different types of materials are used to fill the gap, however lately the two-component grout system is becoming more popular (e.g. Di Giulio et al., 2020; Oggeri et al., 2021; Rahmati et al., 2021). To correctly achieve this, a simultaneous backfilling system and the injected material should satisfy the technical, operational and performance characteristics: the two-component grout must be water-tight, pumpable, workable, able to fill the void, to stiff quickly and to be wash-out resistant, not able to shrink (e.g. Thewes and Budach, 2009; Oggeri et al., 2021).

For these reasons, the open space must be continuously filled during the machine's advancement.

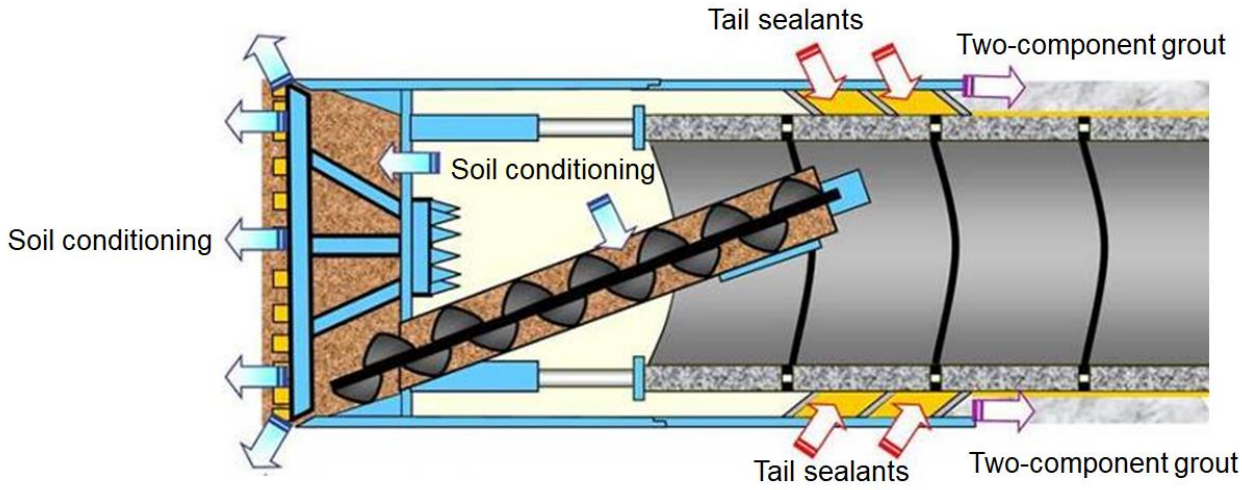

Fig. 1 Section of EPB-TBM with some main aspects highlighted

The mix-design of a two-component grout is claiming for different requirements depending on the job site characteristics and geological formation; however, the typical mix-design in a m^3 system for a two-component grout consists in general by cement (280-450 kg), bentonite (30-60 kg), water (730-860 kg), retarder (3-5 kg) and accelerator (60-80 kg)**,** normally sodium silicate. The accelerator ("B" component) is generally added just before the pumping phase of the mix of water, bentonite, retarder and cement ("A" component). Simultaneous backfilling with two-component grouts, in comparison with the mortar type grouts, keeps in general lower settlements during TBM excavation (Hirata, 1989). Keeping in mind the importance of the two-component grout during tunneling advancement, it must be recognized that not many works deal with this material both experimentally and numerically. It is well-known that the mechanical properties of the two-component grout change based on the mix-design type (e.g. Flores, 2015; Todaro et al., 2019).

Oh and Ziegler (2014), Shah et al. (2018), Ochmański et al. (2018) and more recently Ochmański et al. (2021) performed a numerical analysis regarding the effects of the two-component grout on the tunnel settlement. However, the creep behavior of two-component grouts has not be analyzed in details so far. In this paper, a mix-design of a two-component grout has been tested by determining the Unconfined Compressive Strength (UCS) and the

111 creep strain evolution at varying curing ages. From the analysis of the laboratory results it
112 was possible to understand the behavior of this material with particular attention to the
113 deformability and strength values during a loading phase and the analogous response to
114 long term loading, by maintaining different loads acting on the specimen. It was possible to
115 describe the development of deformations over time of the two-component material
116 subjected to different load entities related to the UCS. From the analysis of the laboratory
117 results it was possible to describe a behavioral model of the creep phase of the two-
118 component material and also to evaluate the effects of the evolution of deformations over
119 time on the behavior of the segmental lining and on the displacements of the tunnel wall.
120 The analysis of a real case of a tunnel excavated in Northern Italy in a weakly cohesive
121 material allowed to verify the effects of the creep of the two-component material on the
122 behavior of the support system, arriving at evaluating the reduction over time of the loads
123 applied to the segmental lining (stress relief) and the increase in the radial displacement of
124 the tunnel wall at the end of the creep phase.

125 **General creep models**

126 Due to the strains increase with time in tunnelling, creep can be an important phenomenon,
127 especially for very soft or heavily fractured rocks under significant in-situ stresses (Yu, 1998;
128 Dusseault and Fordham, 1993), for rocks of argillaceous nature (Barla, 2011) or also when
129 a combination of applied stresses and material properties, some specific geological
130 conditions, and/or a groundwater flow exist. For rocks containing clay, the phenomenon,
131 associated with water migration (or clay platelets orientation), could be considered as a
132 consolidation typology (Goodman, 1980).

133 When a specimen is subjected to a constant maintained load in unconfined compression in
134 the microfracturing range, the specimen will continue to deform after initial application of the
135 load (Hardy et al., 1969). Normally creep strain are not fully recovered; therefore, large

plastic deformations take place (Dusseault and Fordham, 1993). Time dependent strain is much higher in weak rocks and evaporites than in stiffer rocks, but the typical shape of the strain trend is similar. Three reference types of deformation can be observed following the strain trend under a maintained stress (Farmer and Gilbert, 1981):

a) level of applied load is maintained above a critical microcrack development level, then unstable fractures will accelerate creep strains and quickly leading to specimen failure;

b) level of stress is well below the critical microcrack development level, there will be a limited spreading of fractures with an exponentially decaying of the creep strain rate and stable conditions (no failure);

c) the intermediate zone represents a meta-stable condition, where cracks propagation can occur leaving stable microfractures and reaching unstable conditions with crack acceleration and failure. This can happen also with staged conditions of loading (Figure 2, Oggeri, unpublished data).

Figure 2 shows an example of evaporitic rock presented for comparison with different behaviour with deformation under constant loading. Trend of the curves, threshold levels for both stress and strain and final control of specimen integrity can differ during testing. Therefore, a dedicated experimental approach is deemed necessary for any new material. Specimen a) and b) are coming from the same deposit, but even small differences in texture and grain size of particles are influencing the test results.

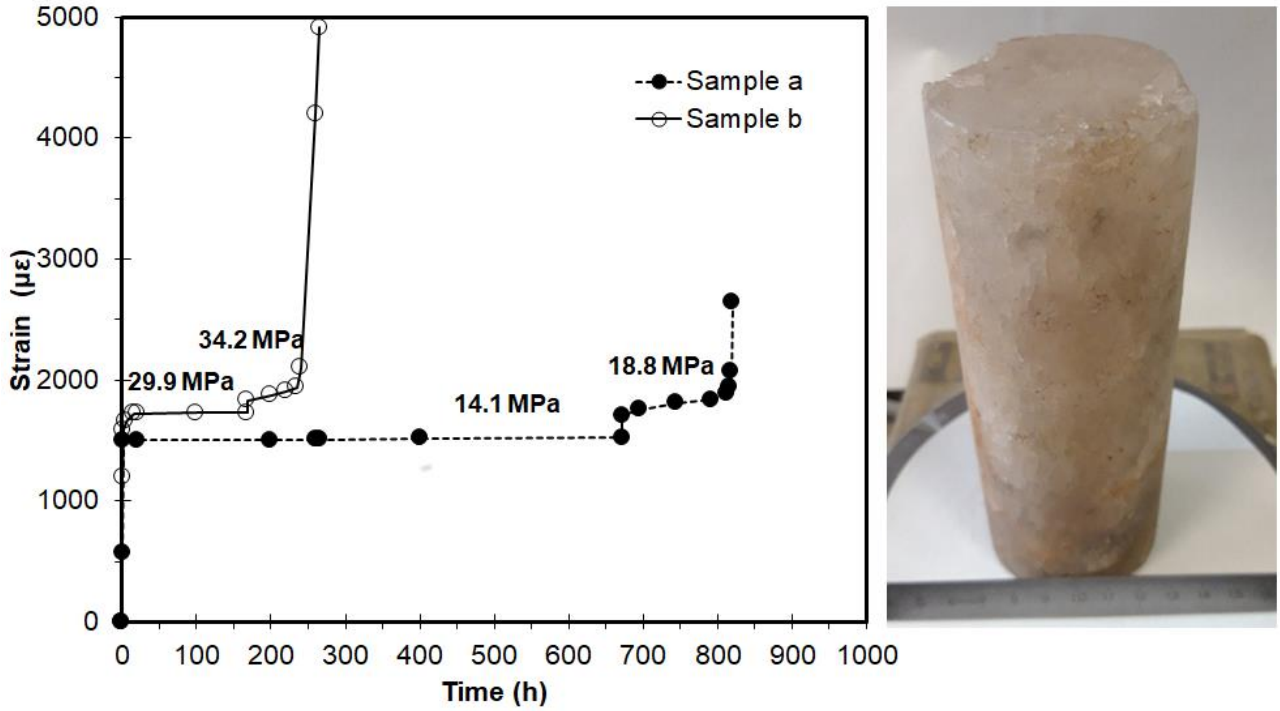

Fig. 2: Two examples of creep with a staged loading on evaporitic rocks. Specimen a) is entirely made of salt, with microcrystals from millimetric to centimetric size (see figure on the right); after an initial stable load at 14.1 MPa, failure is reached with a step at 18.8 MPa. Specimen b) is a fine-grained salt including elements of marl; after an initial load at 29.9 MPa, failure is reached with a step at 34.2 MPa.

Many models of creep and testing procedures have been carried out after the extended research by Griggs (1939) and refinements after Lama and Vutukuri (1978). Alternative approaches have been developed by Price and Farmer (1981).

In tunneling, many models are used to describe the creep of rocks and sprayed concrete, e.g. rheological models (Jaeger and Cook, 1979), Kelvin model (Neville et al. 1983; Jaeger and Cook, 1979; Rokahr and Lux 1987), Burgers model (Yin 1996), viscoplastic model (Thomas 2009). In sprayed concrete creep is significantly higher at an early stage of load as the strength of sprayed concrete is lower, as found by Huber (1991), who observed that a sample loaded at 8 days creeps by 25% more than a similar sample loaded at 28 days.

However, it must be kept in mind that some accelerators increase the early strengths (Melbye 1994) therefore creep after 24 or 48 h is close to that at greater ages (Kuwajima 1999). Besides, studies have been carried out for the assessment of creep reaction of grout for rockbolts (Van der Schyff, 2007), or for a new method for designing the grout mix based on the induced shear stress rather than on the compressive strength (Orumchi and Mojallal, 2017); other contributions have been given for the creep behavior of a grouted sand (Delfosse-Ribey et al., 2006): depending on the nature of the grout, the grouted sand has exhibited creep strains of different degrees; moreover, similarities can be found for both creep behavior and fatigue behavior as found trend curves have shoved similar shapes.

Arnau et al. (2011) provided analyses in order to study the backfill grout behavior and its influence on the longitudinal response of the lining in plane strain. Three different grout moduli of elasticity were used in the analysis for each different ground condition. An assessment of the influence of grout shrinkage was also performed by assuming a value of 0.05 mm/m according to favorable curing conditions. The results showed that the modulus of elasticity of the grout was not presenting a significant influence on the lining axial stress, while tensile cracking for very stiff grouts could occur and that the lining creep and the grout shrinkage were not significantly influencing the grout tensile stress for general tunnel conditions. Backfill grout cracking was unable to influence negatively the radial structural capacity of the segmental lining, while caused a reduction in the water-tightness of the lining. It must be pointed out that in some cases (hydraulic tunnels) there is a significant internal pressure in the tunnel which forces the backfilling mortar to play a crucial role of contact between lining and rock mass. Besides, over time cracks lead to a loss of confinement of the same backfilling material which, consequently, significantly reduces its mechanical characteristics which could also lead to significant alignment/structural problems in the lining.

As final comment, the annulus grout material may remind of clay (bentonite)-cement slurries for diaphragm wall applications (e.g. Cardu and Oreste, 2012; Spagnoli et al., 2016). Although creep behavior may be studied, operative care is focused mainly on integrity, low permeability performances, self-sealing properties, as well local displacement of the structure *in situ*. For the annulus grout loading values are changing together with curing, and stiffness and time performance is governing the interaction between a soft material (usually the ground) and a very stiff material (the concrete segments).

Laboratory creep behavior of the two-component grout

The tested two-component mix-design adopted for this experimental campaign was based on the following parts:

- Part A: water 800 g, bentonite 35 g, cement (CEM I 52.5) 350 g, retarder 17.5 g (solution contains 20% solid therefore retarder dosage by weight of cement is 1%);
- Part B: water glass (sodium silicate) 85 g.

Part B is added at the end of mixing of the mentioned components as it reacts quickly by producing a viscous grout (water glass represents about 7% of added weight to the initial mix). Grout has been prepared starting from the bentonite hydration (duration at least 48 hours), then the slurry has been maintained for another 24 hours at low stirring. The mixing with retarder and cement has been arranged directly inside the casing of the specimens, by manual dispersion; finally, water glass catalyst has been injected into the fluid grout and a high-speed rotating mixer (up to 8000 rpm) has been used during this phase. Every specimen has been prepared by respecting the mass percentages provided for the standard mix; weight of the components has been determined by means of 0.01 g precision scale.

Fast rotation of mixer has allowed to disperse the catalyst and homogenize the grout inside the casing. Then, the casings containing the specimens have been recovered in a box for

curing in water. Curing procedure has been selected following three different timelines for testing: 24 h; 7 days; 28 days. Preparation of the specimen requires great care and repeated preliminary attempts were done in order to obtain a suitable material. Temperature during the tests has been kept constant at 19-21°C.

UCS has been carried out in a Belladonna mechanical press for soils, equipped with bidirectional displacement rate control device. Transducers used to measure load and vertical displacement have been respectively a full bridge load cell (CCT model, full scale 5 kN and precision of 1 N) and LVDT devices (HBM models, precision 0.001 mm). Vertical displacements have been measured following the relative movement of the base of the specimen. Advancing rate has been adapted in the range of 0.15 ÷ 0.45 mm/min and suitable results have been obtained for the range 0.30 ÷ 0.45 mm/min. This selection is a good compromise to avoid creep behavior (excess of lateral swelling) or sudden failure (vertical cracks). Specimen diameter has been selected as 46.5 mm.

Creep testing has been performed by using a standard mechanical oedometer (Belladonna equipment) (Fig. 3), with settings to host the cell (a graduated plastic cylinder) with water and the specimen. The host cell was made of stiff and transparent polypropylene and the contact base with the specimen has been provided of a flat stainless-steel disk to avoid any local deformation. A similar arrangement was already successfully used by Delfosse-Ribey et al. (2006).

The adaptation of a classical Bishop lever oedometer has been done in order to fit the expected strength level of the grout, if compared with typical properties of rock material tested for creep (salt, coal, gypsum etc.). This equipment permits:

- to work from very low to medium stress levels;
- to provide a perfect vertical alignment of caps at the extremities of the specimen;
- to provide a full recovery of mechanical gaps during assembling of specimens;

- an easy water saturation control in open cells and drainage filters at contact with the specimens;
- to continuously read the vertical displacement versus time; easy and direct check of macroscopic cracking growth or lateral bulging.

The procedure for testing is following some steps: 1) preparation of the specimen with selected mix and curing time in submerged conditions; 2) weighting and photos of the specimen; 3) assembling inside the cell and filling of the cell with water; 4) mechanical gap recovery of the displacements of the apparatus; 5) application of the selected load on the lever arm in order to reach the selected stress level, according to previous experience gained in uniaxial compression tests; 6) measurement of vertical displacement versus time; 7) detection of the trend and completion of the testing duration after reaching either a failure (stable failure when residual bearing capacity is evident; unstable failure when specimen start to yield and collapse) or a constant settlement; 8) removal of load and measurement of eventual elastic strain recovery; 9) removal of the specimen, taking photos to verify the crack pattern and weighting for moisture content.

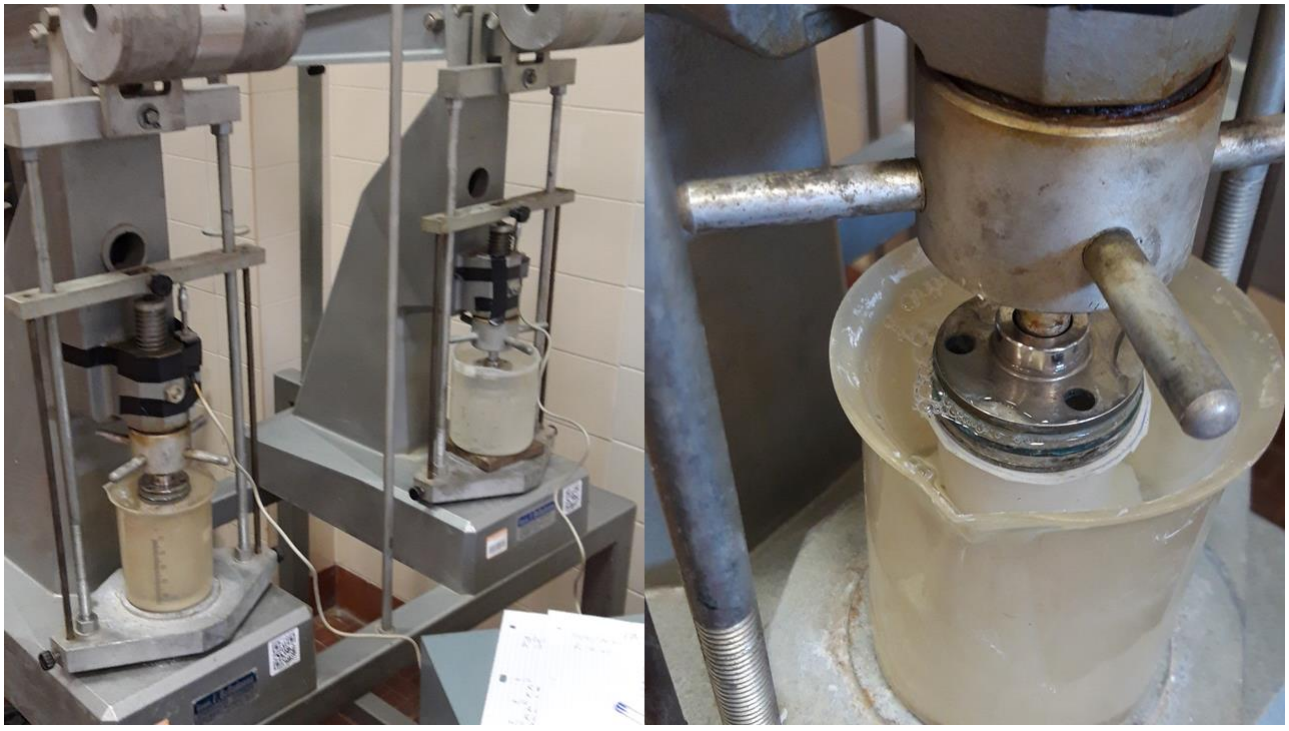

Fig. 3 Left: Twin cells adapted in the oedometer frame, where specimens are kept submerged during constant load application and vertical settlement of the base is continuously measured. Right: detail of a specimen inside a testing cell.

It is important to specify that standard test procedure for one-dimensional consolidation properties of soils have been adapted in order to respect the fact that grout is curing during testing: this is not the case for natural minerals such as salt or gypsum. After some practical preliminary tests, repeatability and representativity have been observed for loading periods of no more than one week after 24 hours of initial curing and of no more than four weeks after 7 days and 28 days form curing beginning. Specimens have been maintained saturated during cycles to avoid cracking, and displacements have been measured by means of potentiometric transducers with precision of 0.01 mm. Fig. 4 shows the specimens used for the tests. Quality in terms of homogeneity and geometry was considered acceptable.

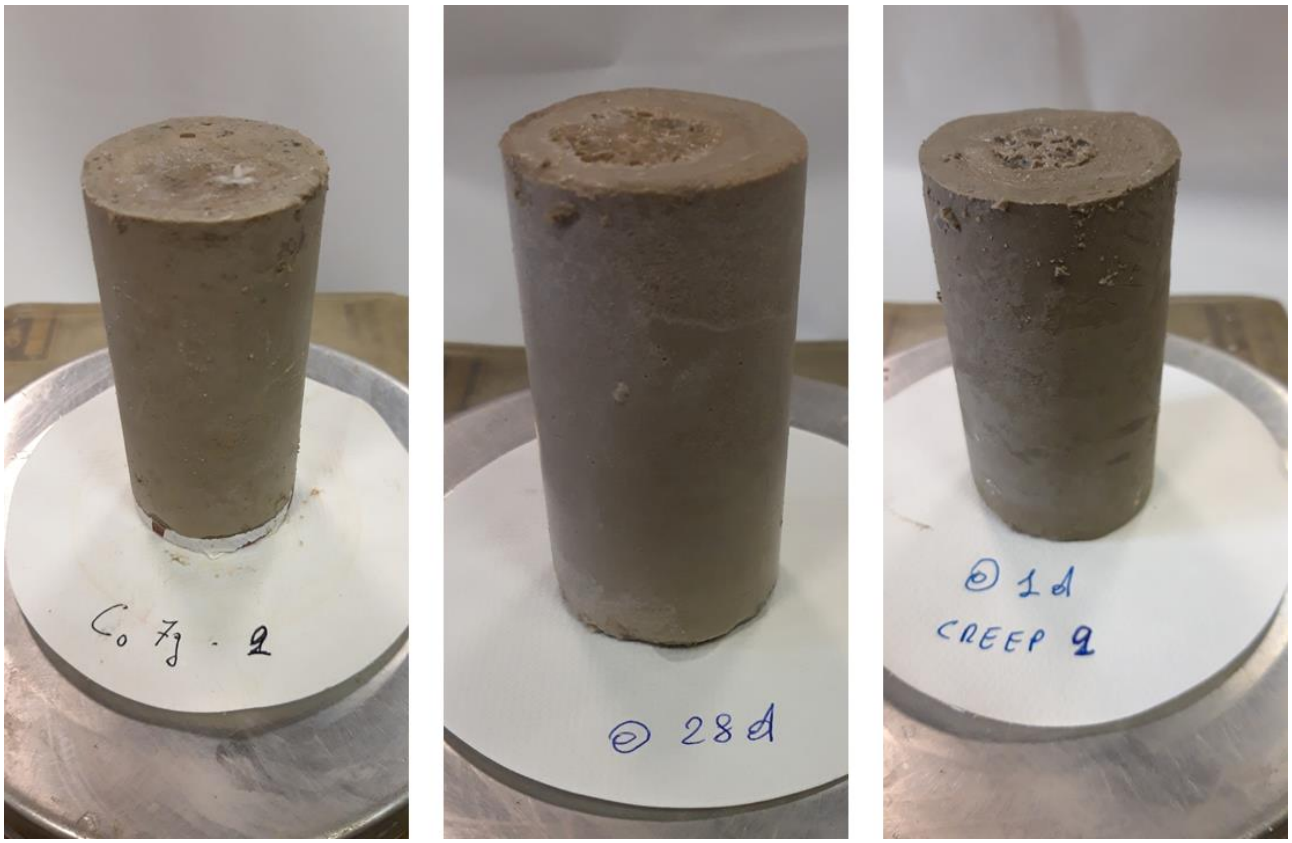

Fig. 4 Example of standard specimens prepared and obtained for UCS and creep testing. The grain size of the cured grout specimens appears regular and homogeneous, without veins or lenses of different consistency.

UCS results

The main results after unconfined compression testing are reported in Table 1. Strength is considered as the maximum value of stress obtained, for the great majority of cases, at yield at the end of the elastic domain. Deformability values are indexed as secant moduli, E_s, at 25%, 50% and 75% of the elastic domain and as tangential values, E_t, at 50% of the elastic domain. In Fig. 5 there is a representative sequence of vertical stress – vertical strain curves for different curing ages. The observed UCS values are rated similar than expected if compared with other available results on this grout type (see Oggeri et al., 2021). Vertical stress versus vertical strain is reliable both in the elastic and in the post peak field. A clear yielding and softening behavior have been observed, with some subvertical and inclined prevailing cracks. In some cases, a pseudo-conical shape at failure has been observed at the extremities of the specimen, thus respecting the ideal Mohr-Coulomb strength criterion (Fig. 6).

291 **Tab. 1 Summary of specimen data for the UCS tests.**

24 h curing	**Diameter (mm)**	**Height (mm)**	**Weight (g)**	**Apparent unit weight (g/cm^3)**	**UCS (kPa)**	**E_s 25% (MPa)**	**E_s 50% (MPa)**	**E_s 75% (MPa)**	**E_t 50% (MPa)**
n.1	46.5	85	187.6	1.299	480	6.5	9.7	11.5	23.1
n.2	46.5	84.4	185.0	1.291	215	5.6	8.7	10.2	17.9
n.3	46.2	85.2	186.2	1.304	350	9	12.3	16.5	26.2
n.4	46.5	84.9	186.3	1.292	320	8.1	10.1	13.3	24.7
7 days curing	**Diameter (mm)**	**Height (mm)**	**Weight (g)**	**Apparent unit weight (g/cm^3)**	**UCS (kPa)**	**E_s 25% (MPa)**	**E_s 50% (MPa)**	**E_s 75% (MPa)**	**E_t 50% (MPa)**
n.1	46.5	86	190.1	1.302	1270	25.8	34.1	42.6	78.1
n.2	46.5	86	192.0	1.314	1110	17.5	26.5	32.3	73.8
n.3	46.5	83	186.3	1.322	760	51.2	63	74.7	76.41
n.4	46.5	84	190.1	1.332	1150	38.5	50	55.4	117.8
n.5	46.5	89	192.6	1.274	990	33.3	43.2	54.6	109.9
28 days curing	**Diameter (mm)**	**Height (mm)**	**Weight (g)**	**Apparent unit weight (g/cm^3)**	**UCS (kPa)**	**E_s 25% (MPa)**	**E_s 50% (MPa)**	**E_s 75% (MPa)**	**E_t 50% (MPa)**
n.1	46.5	83	183.3	1.300	1290	37.8	44.8	54.9	109.4
n.2	46.5	83	185.5	1.316	1110	20.4	26.2	32.7	63.3
n.3	46.5	84	188.6	1.322	1290	33.3	44	59.6	108.7
n.4	46.5	86	192.1	1.315	1400	30.1	43.1	57.1	111.2

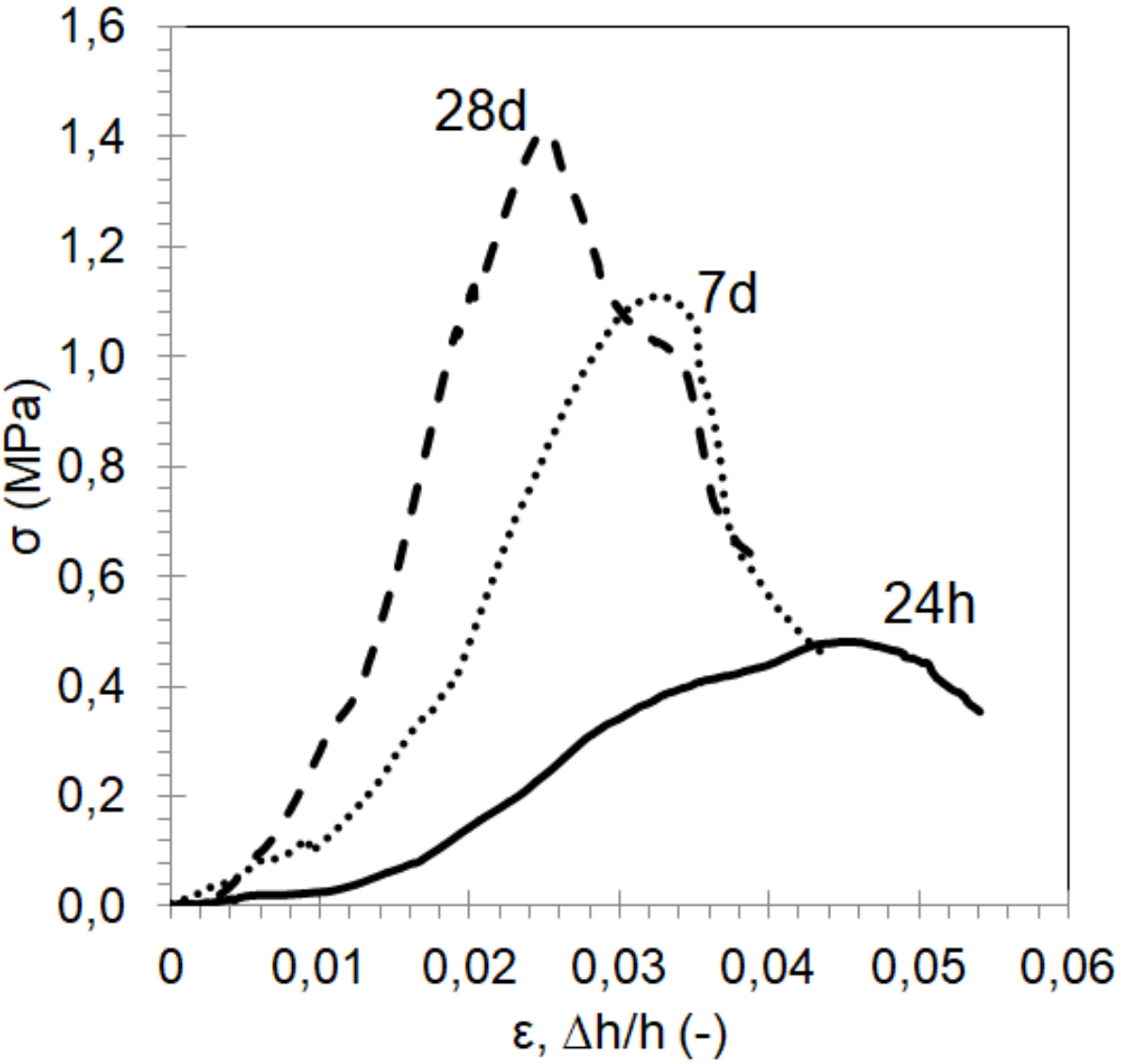

Fig. 5. Examples of vertical stress – vertical strain curves for grout specimens at different curing age (at 24 hours, 7 days and 28 days from curing beginning, respectively), during a uniaxial compressive test. Along the vertical axis applied stress σ in MPa is reported, along horizontal axis induced vertical strain in ε (ratio of the vertical displacement on the sample height) is reported. Strain softening after the stress peak is more evident for short age curing specimens.

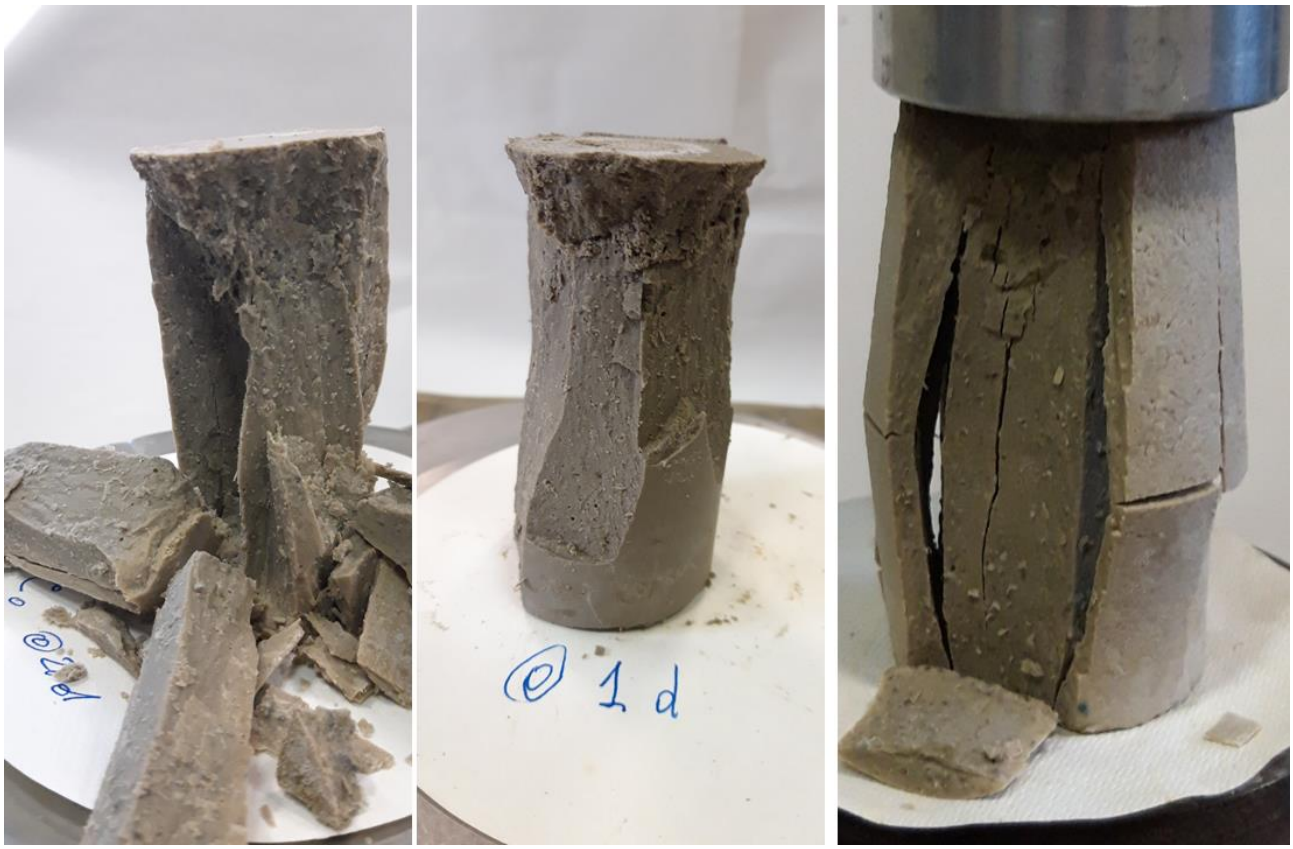

Fig. 6. Different failure modes for specimens after unconfined compression testing. The formation of conical shaped bodies is clearly visible at left and in the middle. On the right, the radial expansion has prevailed with symmetrical formation of vertical slabs.

Creep tests results

Constant loading testing has been carried out on several specimens, and the selection of regular behavior has been reported after exclusion of not homogeneous materials. In Table 2 the evidence of 11 tests is reported, with geometrical data and the applied vertical load**s**, both effective and as a percentage of the reference value obtained from the compression tests. The UCS has been determined in advance in order to properly assign a reasonable ratio of the applied constant load, just because this ratio triggers the passage between a stable and an unstable behavior.

Tab. 2. Summary of specimen data for constant loading (creep) tests. Last column shows the load percentage referred to a representative value of UCS for the same type of grout and curing age.

24 h curing	**diameter (mm)**	**height (mm)**	**weight (g)**	**apparent unit weight (g/cm^3)**	**σ creep (kPa)**	**σ creep (as % UCS)**
n.1 creep	46.2	85.3	187.1	1.308	290	75
n.2 creep	46.5	85.2	186.2	1.287	230	60
n.3 creep	46.5	85.8	187.2	1.285	175	45
n.4 creep	46.5	87.6	189.2	1.270	115	30
7 days curing	**diameter (mm)**	**height (mm)**	**weight (g)**	**apparent unit weight (g/cm^3)**	**σ creep (kPa)**	**σ creep (as % UCS)**
n.1 creep	46.5	87.0	192.0	1.300	700	66
n.2 creep	46.5	85.6	187.9	1.293	580	55
n.3 creep	46.5	93.8	203.8	1.279	460	45
n.4 creep	46.5	85.7	188.5	1.295	350	33
28 days curing	**diameter (mm)**	**height (mm)**	**weight (g)**	**apparent unit weight (g/cm^3)**	**σ creep (kPa)**	**σ creep (as % UCS)**
n.1 creep	46.5	86.0	192.2	1.316	930	75
n.2 creep	46.5	85.1	189.4	1.312	700	55
n.3 creep	46.5	84.2	186.0	1.304	460	35

317 In Fig. 7 the net settlement versus time trend is reported, for the three selected curing
318 periods, respectively 1 day (A), 7 days (B) and 28 days (C). The tests have shown,
319 depending on the applied load magnitude:

320 • at 1 day of curing: a stable behavior for 2 specimens, a stable failure for 1 specimen,
321 an unstable failure for 1 specimen;

322 • at 7 days of curing: a stable behavior for 1 specimen, a stable failure for 1 specimen,
323 and unstable failure for 2 specimens;

324 • at 28 days of curing: a stable behavior for 2 specimens, an unstable failure for 1
325 specimen.

326 Fig. 8 shows some representative effects after the end of the creep test. It is possible to
327 observe how the grout can respond to a constant loading. It is necessary to remind that for
328 1 days and 7 days curing ages grout is still strengthening, even if failures occur due to
329 loading. Only for long term-curing, i.e. 28 days, it fair to state that full mechanical properties
330 of grout have been reached.

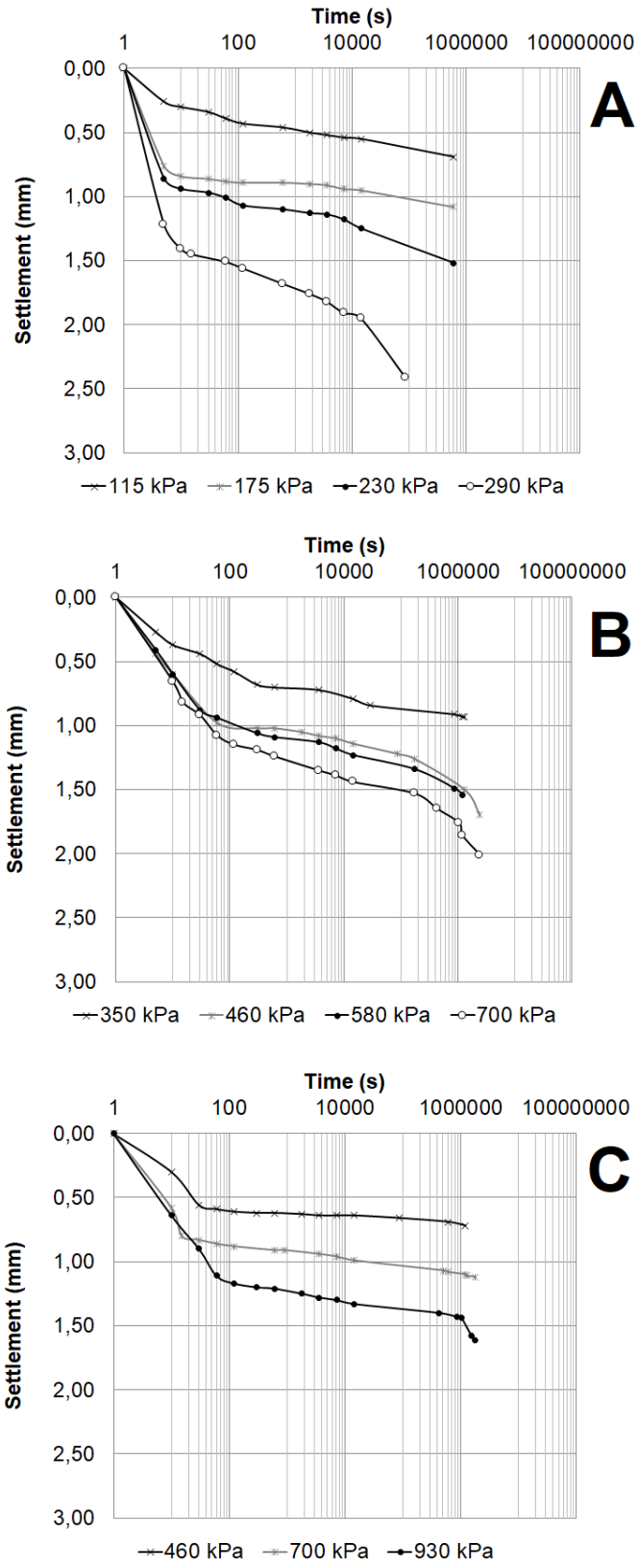

331

332 **Fig. 7 Net settlement versus time are reported, for the three selected curing periods,**

333 **respectively 1 day (graph A with 2 stable behavior, 1 stable failure, 1 unstable failure);**

7 days (graph B with 1 stable behavior, 1 stable failure, 2 unstable failure); 28 days (graph C with 2 stable behavior and 1 unstable failure).

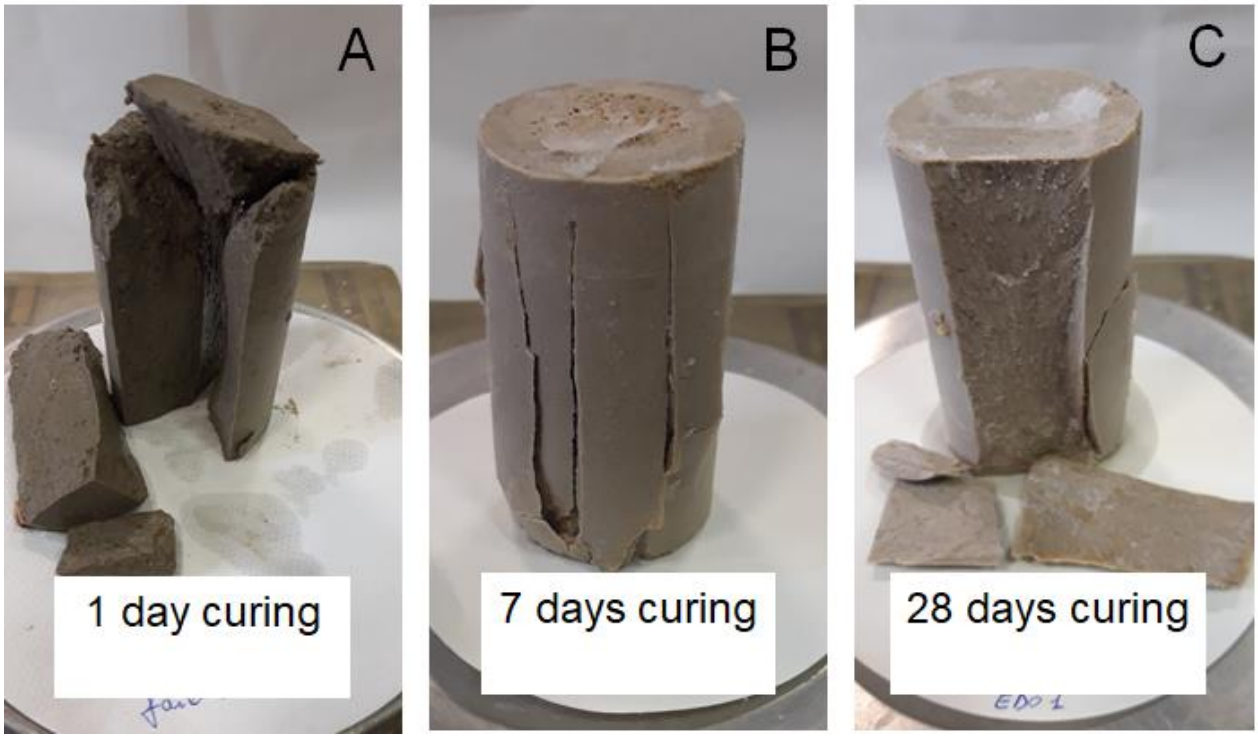

Fig. 8. Different failure modes for specimens after creep (constant load). A) de-assembled specimen, failure with conical end shape, curing 1 day; B) failure with axial symmetry for lateral expansion, 7 days curing; C) failure with conical end shape, 28 days curing.

Comments of laboratory results

The available data and the observed behavior during the standard compression test and during compression tests with constant loads (creep tests), for this mix-design, can allow to put in evidence some features:

- the mixing procedure carried directly inside the casing has determined a little increase in the unit weight referred to the test results reported in a previous campaign, thanks

to the reduction of the weak material removal from the end of the specimen during preparation;

- there is a general increase in UCS strength and in elastic moduli due to the previous point;
- all specimens have shown a post peak behavior, with wider strain softening for shorter curing ages;
- in some cases, a clear evidence of conical shaped ends at failure of the specimens has been observed, both in compression test**s** and during creep test**s**;
- long term strains do not reach an ultimate value, even when in stable loading; this happens in particular at 1 day and 7 days of curing, less for 28 days of curing. The balance between the maintained load and residual strengthening appears to be reasonably the cause for the observed trend;
- strain creep diagrams show one half of final value occur in the initial 2 minutes; there is an initial link with expected values after compression testing, then stiffness changes as a consequence of induced damage. The load in creep tests, even if less than UCS, is anyway applied instantly;
- in creep testing, for some specimens, failure has been observed as a progressive trend towards unstable crack propagation;
- no absolute and unique link between measured settlements in creep and the correspondent modulus of deformability in the compression test has been found; however satisfactory correlations exist between ΔH_{final} in stable creep zones and E_s 75% from compression tests for 1 day and 28 days of curing; in a similar way, correlation exists between $\Delta H_{primary}$ in creep and E_s 75% from compression tests for 7 days of curing;
- the deformative process results to be different for short grout curing age (1 day) respect to 7 or 28 days of curing age;

- Although temperature has an effect on creep behavior for both rocks (Li et al., 2019) and concrete (e.g. Geymayer, 1970) accelerating creep, its effects are beyond the scope of this research.

The trend of deformations over time after 7 and 28 days of curing is interesting to evaluate in order to study the effect of the creep of the two-component material on the behavior of the support system.

In particular, after 7 days of curing it is useful to refer to the curve obtained by applying an axial load equal to 33% of the failure stress (UCS) of the material (Fig. 9); this load did not cause the material to fail and a final stabilization of deformations was observed. For applied loads equal to 45% of UCS or higher (55% and 66%), on the other hand, the failure of the material was achieved after a creep phase.

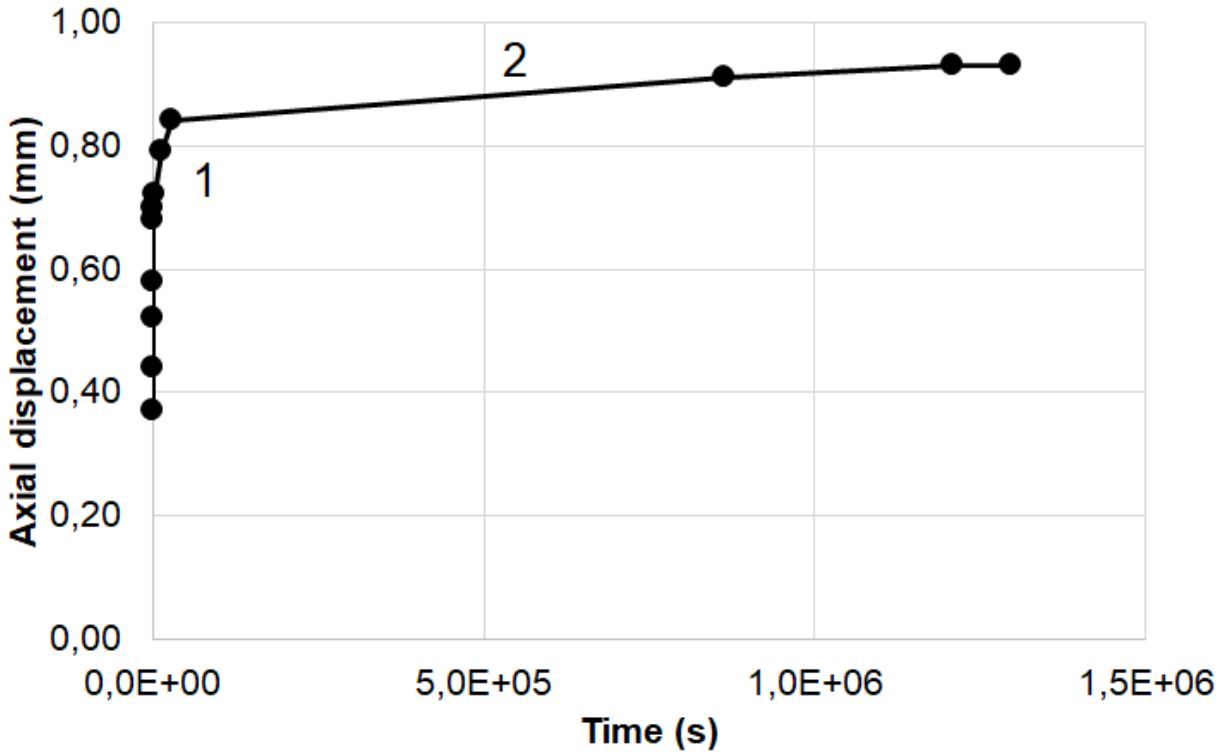

Fig. 9. Trend of deformations over time in a sample of two-component material cured for 7 days and subjected to an axial load equal to 33% of UCS. After the application of the load, there is a significant increase in displacements in the first 10 minutes,

after which the displacements grow with a markedly bi-linear trend (zones 1 and 2 in the graph) until stabilization is reached after about 14 days from loading.

From the analysis of the figure it can be seen that the immediate displacement (δ_{inst}) upon application of the load is 0.37 mm. In the first 10 minutes there is a significant increase in the displacements until reaching a double value of δ_{inst}, after which the displacements increase with a markedly bi-linear trend until stabilization is reached after about 14 days from loading: in the first linear section, the displacement changes from 2.00·δ_{inst} to 2.25·δ_{inst} after 8 hours from the application of the load; in the second linear section it reaches a displacement of 2.50·δ_{inst} after 14 days from the application of the load. The expressions that describe the trend of the displacements over time in the two linear sections are shown below:

$\delta = \left[2.00 + 0.032 \cdot \left(t - {}^{1}/_{6}\right)\right] \cdot \delta_{inst}$ (t in hours), for t ranging between 1/6 hours and 8 hours (1)

$\delta = \left[2.25 + 0.018 \cdot \left(t - {}^{1}/_{3}\right)\right] \cdot \delta_{inst}$ (t in days), for t ranging between 1/3 days and 14 days (2)

After 28 days of curing, the specimen on which a load equal to 75% of the UCS value was applied reached failure after the creep phase. While for loads equal to 35% and 55% of UCS, there was no failure of the specimen subjected to the creep test. More specifically, for the load equal to 35% of UCS we note the same bi-linear trend observed for the case referred to the 7-day curing, with a value of δ_{inst} equal to 0.30 mm. While for the load equal to 55% there is also a bi-linear trend but with the following characteristics: even now in the first 10 minutes there is a significant increase in displacements until reaching a value of 1.5·δ_{inst}; after which the displacements increase up to 1.75·δ_{inst} after 8 hours from the application of the load and in a second stretch up to the final stabilization at 14 days from the application of the load with a final displacement value equal to 2·δ_{inst}.

From a detailed analysis of the results of the creep tests, therefore, the following can be noted:

- the maximum percentage of the load with respect to UCS that would allow to avoid the failure of the specimen in the long term goes from about 40 for 1 week of curing of the material to about 70 for 4 weeks of curing of the specimen;
- the trend of deformations over time follows a bi-linear law after the first 10 minutes of loading; a first stretch is between 10 minutes and 8 hours from the application of the load, the second stretch from 8 hours to 14 days from the application of the load;
- the curing age of the specimen does not seem to alter the deformation curve over time; a certain effect on this curve is given by the applied load, evaluated as a percentage of the UCS value;
- the deformation increases according to two linear sections and the total value of the creep strain is constant and equal to one half of the immediate deformation detected on the specimen upon application of the load, regardless of the curing age of the specimen and the percentage value of the applied load;
- in the first 10 minutes from the application of the load the deformations grow rapidly until reaching 2 times the immediate deformation ($2\cdot \delta_{inst}$) for percentages of the load equal to about 35% of UCS and 1.5 times the immediate deformation ($1.5\cdot\delta_{inst}$) for percentages of the load equal to about 55% of UCS.

Immediate deformation therefore has a significant importance in understanding the phenomenon of creep because it influences the deformation levels that develop in the material over time. From the results obtained in the laboratory tests (uniaxial compression and creep), it can be seen how the initial deformation can be estimated with a good approximation by adopting the tangent elastic modulus determined in the uniaxial compression tests, associated with the stress value equal to the applied load in the creep

test. Ultimately, if the applied load is equal to 35% of UCS, the immediate deformation of the specimen ε_{inst} will be defined by the following relationship:

$$\varepsilon_{inst} = \frac{0.35 \cdot UCS}{E_{t,35\%}} \quad (3)$$

where:

UCS is the monoaxial compressive strength of the two-component material measured for a specific curing age;

$E_{t,35\%}$is the tangent modulus of elasticity measured at a stress level equal to 35% of UCS, evaluated on a specimen of two-component material with a specific curing age, subject to the uniaxial compression test.

Analysis of the effects of creep on the tunnel support system

The support system (segmental lining with the two-component material surrounding it) has been studied in detail by Oreste et al. (2021). Using the convergence-confinement method, it is possible to analyze the interaction between this support system and the tunnel wall. It is a very widespread analytical method in the geomechanical field, such as the limit equilibrium method (LEM) (Oreste, 2013), which combines the advantage of the simplicity of the approach with the precision and reliability of the results.

Some simplifying hypotheses are necessary (Osgoui and Oreste, 2007; Oreste, 2009a; 2009b; Ranjbarnia et al., 2014; 2016; Spagnoli et al., 2016):

- circular and deep tunnel;
- initial stress state of hydrostatic type (k_0 = 1);
- homogeneous and isotropic soil or rock, with linear elastic behavior.

Specific and detailed studies of the behavior of the support system can be developed by adopting three-dimensional numerical modeling (Do et al., 2014; 2015a; 2015b: Pelizza et al., 2000).

In order to evaluate the load applied on the segmental lining and the deformation conditions of the tunnel wall and of the segmental lining, it is necessary to intersect the convergence-confinement curve with the reaction line of the support system (Fig. 10) (Oreste, 2003).

The convergence-confinement curve depends on the behavior of the ground at the tunnel boundary: it relates the internal pressure applied on the tunnel wall to the radial displacement of the tunnel wall towards the center of the tunnel (Brown et al., 1983; Panet, 1995). As the internal pressure decreases, the radial displacement increases, until it reaches the maximum value when the internal pressure is zero.

The reaction line of the support system relates the pressure applied by the support system to the variation of the displacement of the tunnel wall. This displacement also corresponds to the displacement manifested by the support system on its outer edge, which comes into contact with the tunnel wall. As the movement of the tunnel wall increases, the pressure applied by the tunnel wall will increase.

There is an end equilibrium point between the tunnel and the support system which is given by the intersection between the convergence-confinement curve and the reaction line of the support system.

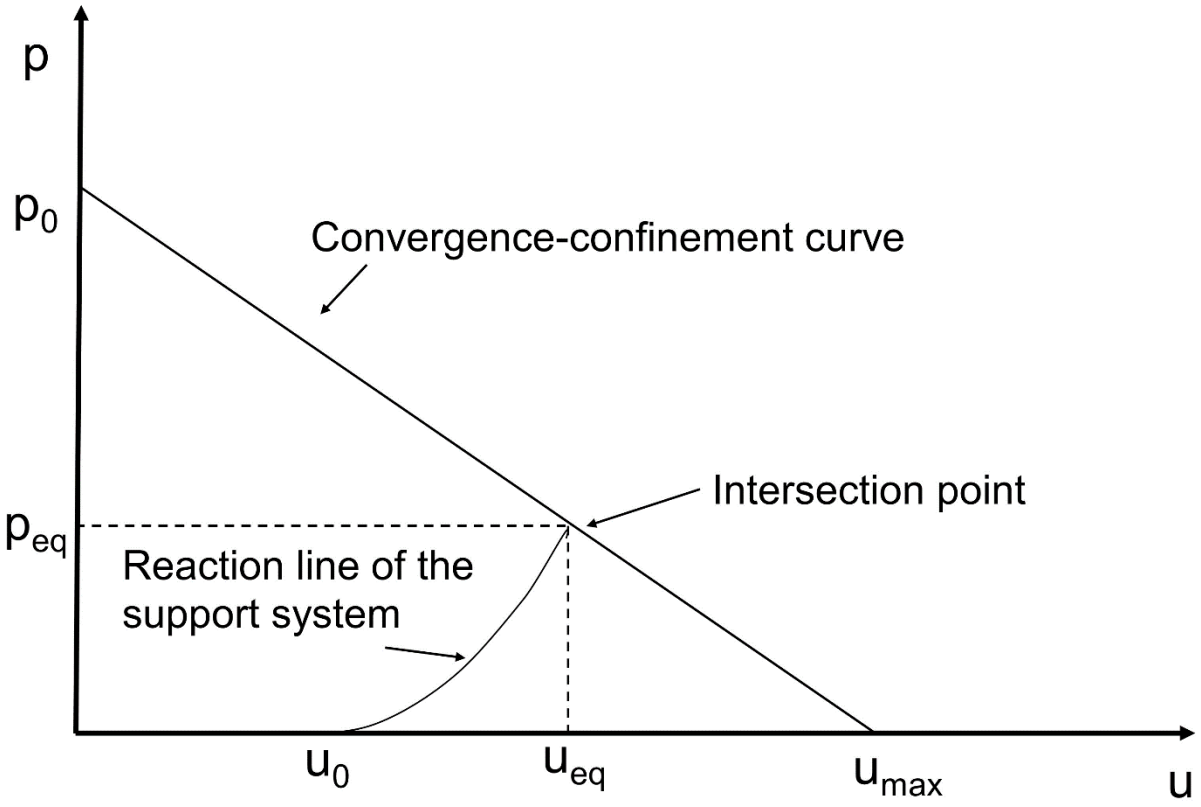

Fig. 10 The intersection between the convergence-confinement curve of the tunnel and the reaction line of the support system when this is composed of segmental lining and the two-component material around it (modified by Oreste et al., 2021). Legend: p: internal pressure applied to the tunnel wall; u: radial displacement of the tunnel wall; p_0: lithostatic stress in the soil or rock at the depth of the tunnel; u_0: displacement of the tunnel wall at the distance from the excavation face of the section where the support system is installed; $u_{max} = (1 + \nu_{gr}) \cdot p_0 \cdot R/E_{gr}$, where E_{gr} is the elastic modulus and ν_{gr} the Poisson's ratio of the ground (soil or rock) present around the tunnel; R is the tunnel radius; p_{eq} and u_{eq}: respectively the load applied on the support system and the radial displacement of the tunnel wall in the final condition of equilibrium, at the end of the process of loading the support system.

An iterative procedure was developed to correctly describe the reaction line of the support system (Oreste et al., 2021). The curvilinear shape of the reaction line is due to the fact that

the two-component material matures during the loading of the support system. There will be two specific different stiffnesses of the support system: when the segmental lining is installed, the two-component material will have a very low initial stiffness (short curing age); at the end of the support loading process (when the excavation face has advanced to a distance of about $4 \cdot R$ from the study section), the stiffness of the two-component material reaches its maximum value. This different stiffness of the support system is reflected in the inclination of the curvilinear reaction line, which initially presents a lower tangent, until reaching the maximum inclination of the tangent line near the point of intersection with the convergence-confinement curve (end of the support system loading process).

The point of intersection is given by the values p_{eq} and u_{eq} respectively the load applied on the support system and the radial displacement of the tunnel wall in the final equilibrium condition. p_{eq} and u_{eq} can be obtained from the following expressions:

$$u_{eq} = \frac{2 \cdot p_0 + u_0 \cdot \left(k_{sys,fin} + k_{sys,in}\right)}{\frac{2 \cdot E_{gr}}{(1+\nu_{gr}) \cdot R} + \left(k_{sys,fin} + k_{sys,in}\right)} \quad (4)$$

$$p_{eq} = p_0 - \frac{E_{gr}}{(1+\nu_{gr}) \cdot R} \cdot u_{eq} \quad (5)$$

where:

$k_{sys,in}$ and $k_{sys,fin}$: stiffness of the support system at the beginning and at the end of the loading process; for the evaluation of the initial stiffness, reference is made to the curing age t_0, necessary to resume the advancement of the TBM machine, which marks the start of loading of the lining; for the evaluation of the final stiffness, reference is made to the time (t_f) necessary for the excavation face to reach a distance of about $4 \cdot R$ from the studied section.

The overall stiffness of the support system is evaluated using the following equation (Oreste, 2003; Oreste et al., 2021):

$$k_{sys} = \frac{2 \cdot E_{fm} \cdot (1-\nu_{fm}) \cdot R \cdot \left[\frac{E_{fm}}{(1+\nu_{fm})} + (R-t_{fm}) \cdot k_{sl}\right]}{E_{fm} \cdot (1-2 \cdot \nu_{fm}) \cdot R^2 + (R-t_{fm})^2 \cdot \left[E_{fm} + (1-2 \cdot \nu_{fm}) \cdot (1+\nu_{fm}) \cdot k_{sl} \cdot t_{fm} \cdot \left(1 + \frac{R}{(R-t_{fm})}\right)\right]} - \frac{E_{fm}}{(1+\nu_{fm}) \cdot R} \quad (6)$$

where:

$$k_{sl} = \frac{E_{sl}}{(1+\nu_{sl})} \cdot \frac{(R-t_{fm})^2 - (R-t_{fm}-t_{sl})^2}{(1-2 \cdot \nu_{sl}) \cdot (R-t_{fm})^2 + (R-t_{fm}-t_{sl})^2} \cdot \frac{1}{(R-t_{fm})}$$

k_{sl} is the radial stiffness of the segmental lining;

E_{fm} and ν_{fm} are respectively the elastic modulus and the Poisson's ratio of the filling material; E_{fm} varies over time with increasing curing age;

E_{sl} and ν_{sl} are respectively the elastic modulus and the Poisson's ratio of the segmental lining;

t_{fm} and t_{sl} are respectively the thickness of the filling material and of the segmental lining.

To determine the k_{sys} values it is necessary to evaluate the elastic modulus of the filling material E_{fm}. Imagining a progressive loading over time with a regular advancement of the excavation face, the deformation process that develops in the filling material is the one that refers to the first minutes of the creep tests.

Therefore, for the evaluation of the $k_{sys,in}$ reference must be made to the initial tangent elastic modulus ($E_{fm} = E_{t,0\%}$ of the filling material). To determine $k_{sys,fin}$ a value of the elastic modulus of the filling material must be adopted which depends on the stress level reached inside it in the final equilibrium condition:

$$E_{fm} \cong \frac{E_{t,\alpha}}{\omega} \quad (7)$$

where:

535 $E_{t,\alpha}$ is the tangent elastic modulus of the filling material associated with a percentage load
536 level α referred to UCS;

537 ω is a correction coefficient that takes into account the deformation increase that occurs in
538 the first 10 minutes of load in the creep test; it depends on the percentage α of the stress
539 level acting in the filling material with respect to the UCS strength, i.e. $\omega = 2.875 - 2.5 \cdot \alpha$.

540 Since the stress state induced in the filling material depends on the still unknown value of
541 p_{eq}, also in this case the value of E_{fm} must be adapted as a function of p_{eq} and u_{eq}, which
542 is obtained from the intersection of the two curves. Another iterative procedure is therefore
543 necessary.

544 The value of the maximum principal stress in the filling material can be obtained from the
545 following expression (Oreste et al., 2021):

546 $$\sigma_{1,max,fm} \cong \frac{u_{eq} \cdot \frac{E_{fm}(t_f)+E_{fm}(t_0)}{2 \cdot R} + \left(\nu_{fm}+\nu_{fm}^2\right) \cdot p_{eq}}{\left(1-\nu_{fm}^2\right)} \quad (8)$$

547 where: $\sigma_{1,max,fm}$ is the maximum (circumferential) principal stress in the filling material.

548 The value α will be adapted until the values of p_{eq}, u_{eq}, $\sigma_{1,max,fm}$ and UCS are compatible
549 with each other. At that point, the reaction line of the support system can be correctly placed
550 in the graph and p_{eq} and u_{eq} evaluated.

551 Once the final configuration of the support system has been reached, it will be possible to
552 represent the effect of the creep on the bilinear tract of Fig. 9. On the basis of the
553 experimentation carried out and what was deduced in the previous paragraph, the overall
554 deformation increase due to the creep phenomenon can be estimated as half of the
555 immediate deformation, regardless of the curing age of the specimen and the value of the
556 applied load. It is therefore possible to derive the increase in deformation due to the creep
557 in the filling material from the following expression:

$$\varepsilon_{creep} = 0.5 \cdot \frac{\sigma_{1,max,fm}}{E_{t,\alpha}} \quad (9)$$

Since this deformation ε_{creep} is a circumferential deformation at the extrados of the filling material ring, it is possible to derive from it the increase in displacement Δu of the tunnel wall:

$$\Delta u = \varepsilon_{creep} \cdot R \quad (10)$$

Thanks to the knowledge of Δu it will be possible to represent the effect of the creep of the filling material on the graph of the convergence-confinement curve and evaluate the final displacement of the tunnel wall (Fig. 11).

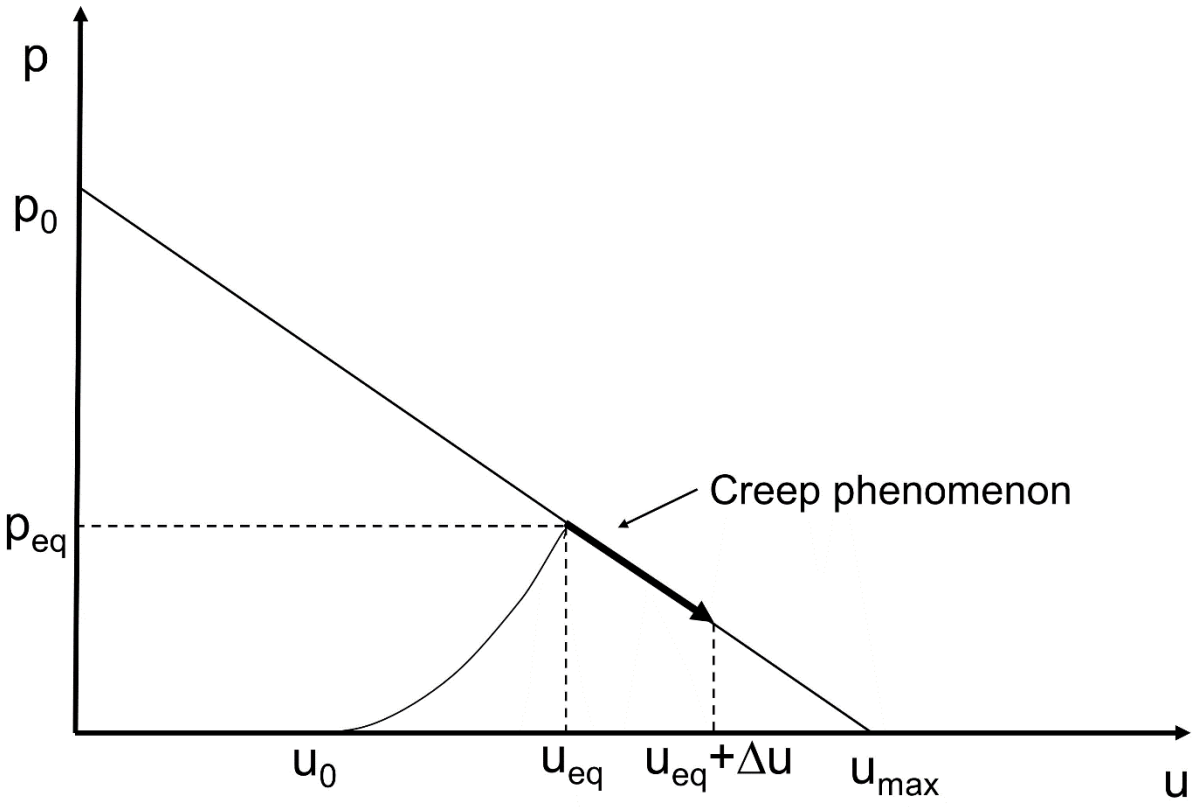

Fig. 11. Representation of the creep phenomenon in the filling material once the final equilibrium point is reached at the end of the process of placing the support system in charge. Legend: Δu: increase in the radial displacement of the tunnel wall due to the creep of the filling material.

The creep phenomenon therefore produces an increase in the displacement of the tunnel wall, as well as a stress discharge of the segmental lining. Both results are fundamental for tunnel design. The increase in the displacement of the tunnel wall is useful for evaluating the subsidence of the soil surface in the long term. The stress relief of the segmental lining allows to obtain the correct value of the safety factor of the support system in the long term. Furthermore, the increase in the displacement of the tunnel wall as a result of the creep can lead to values exceeding the maximum acceptable limits, such as to indicate an incorrect functioning of the tunnel-support system. The final control of this displacement in the tunnel design stage, therefore, is essential to avoid excessive values which could lead to high risks of instability of the tunnel.

Example of support system design considering the filling material creep phenomenon

In defining the thickness of the filling material and also the thickness of the segmental lining, it is necessary to consider the evolution over time of the mechanical characteristics of the filling material (following its curing) and the creep phenomenon. In fact, the curing over time and the creep phenomenon markedly characterize the two-component material and influence the loading of the support system. The final load acting on the segmental lining, therefore, depends on the thickness of the filling material and on the methods of loading the support system. Oreste et al. (2021) have already demonstrated how the thickness of the filling material, the downtime of the TBM machine after the construction of the support system, the average speed of advancement of the TBM after the stop of the TBM are all elements that influence the stress state in the filling material and the load acting on the support system.

More specifically, the case of a tunnel with a length of 5 km and a diameter of 9.4 m, excavated at a depth of about 70 m (p_0 = 1.12 MPa) in Northern Italy by a TBM machine (EPB type) in a weakly cohesive soil having an elastic modulus E_{gr} of 150 MPa and a

Poisson's ratio v_{gr} of 0.3 was analyzed in detail. The thickness adopted for the segmental lining (t_{sl}) was 0.35 m, the thickness of the filling material (t_{fm}) was 0.15 m. For the segmental lining concrete, an elastic modulus E_{sl} of 30,000 MPa and a Poisson's ratio v_{sl} of 0.15 were assumed.

Considering a still stand for the construction of a new lining ring of 1 hour at a distance of 2.5 m from the excavation face and an average advancement speed of the TBM v of 0.35 m/h, the reaction line of the reported support system is shown in Figure 12 (modified after Oreste et al., 2021).

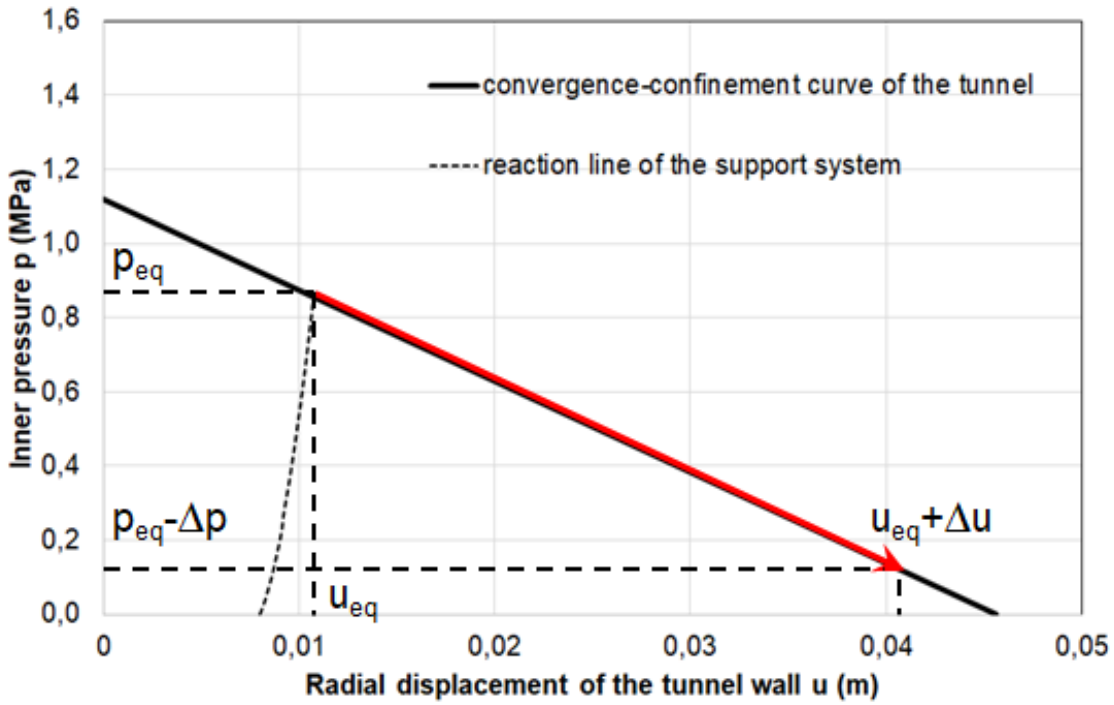

Fig. 12. Convergence-confinement curve of the tunnel and reaction line of the support system in the examined case: tunnel with a diameter of 9.4 m at a depth of 70 m excavated in a weakly cohesive soil with an elastic modulus E_{gr} of 150 MPa. The support system consists of a 0.35 m thick segmental lining and a 0.15 m thick filling material ring. The red line represents the modification of the equilibrium point on the

convergence-confinement curve following the creep phenomenon in the filling material.

The pressure p_{eq} associated with the intersection point is 0.86 MPa and represents the load acting on the support system at the end of the loading process, when the excavation face reaches a distance of about $4 \cdot R$ from the study section of the support system. The displacement u_{eq} is 10.7 mm: it is the final displacement of the tunnel wall at the end of the loading process.

Using eq. 8 it is possible to determine $\sigma_{1,max,fm}$, the maximum (circumferential) principal stress in the filling material at the end of the loading of the support system; a value of 0.92 MPa is obtained, which constitutes 31.6% of the strength of the material after about 48 h, the average time necessary to reach the distance of $4 \cdot R$ from the investigated section.

From the experimental study developed and presented in the previous paragraphs, it was possible to verify how the long-term strength of the two-component material is only a percentage η of the UCS. In particular, the value of η depends on the days of curing of the material:

$$\eta \cong 0.3 + 0.0143 \cdot t_c \tag{11}$$

Where:

t_c is the curing age in days**.**

After two days of curing (48 h), therefore, η worth about 32.9%. This means, therefore, that a maximum stress of 0.92 MPa (31.6% of the compressive strength UCS) is bearable by the two-component material even in the long term without reaching failure. By maintaining its integrity, the two-component material is able to effectively perform the task of transferring

632 the radial loads to the segmental lining and allowing the support system to be waterproofed,
633 preventing water from infiltrating inside the tunnel.

634 As for the deformation increase of the tunnel wall, the value of Δu can be determined on the
635 basis of equations 9 and 10 and considering that the stress $\sigma_{1,max,fm}$ inside the two-
636 component material tends to decrease progressively during the creep phase: it is therefore
637 necessary to adopt the average value that this stress assumes in this specific phase.
638 Therefore, assuming a tangent elastic modulus E_t at two days of curing equal to 40 MPa,
639 we obtain a ε_{creep} value of 0.0067 and an increase in the radial displacement of the tunnel
640 wall of about 31 mm. This increase in the deformations of the tunnel wall has the effect of
641 reducing the load applied on the segmental lining from the initial value of 0.86 MPa to the
642 final value (at the end of the creep phase) of 0.11 MPa. A consistent reduction of the acting
643 loads and of the stress state induced in the concrete which is often found when detailed
644 measures for monitoring the behavior of the segmental lining are available long times after
645 its installation.

646 **Conclusions**

647 The filling material inserted in the gap between the segmental lining and the tunnel wall has
648 several important roles aimed at ensuring the effectiveness of the support system of a tunnel
649 excavated with a TBM machine. Nowadays a **bi**-component filling material is widely used,
650 which has particular characteristics: a curing phase during which the mechanical parameters
651 evolve rapidly; a creep behavior with secondary deformations that develop over time when
652 the material is subjected to a stress load. These features make the interaction between the
653 support system and the tunnel complex, given that the filling material is loaded progressively
654 over time, starting from its installation into the gap between the segmental lining and the
655 tunnel wall. The creep phase generally comes into play at the end of the support system

loading phase and has as a consequence the reduction of the loads transmitted to the segmental lining and the increase in deformations of the tunnel wall.

The creep phenomenon has been studied for many other materials in the field of geotechnics and geomechanics. Many models have been developed and are known in the scientific literature to represent the behavior of such materials. Although the two effects mentioned above and induced by the creep of the filling material on the extrados of the segmental lining are very important, no studies on this topic are available in the literature.

In particular, the increase in the radial displacement of the tunnel wall due to the phenomenon of creep in the filling material can induce high subsidence on the soil surface and can lead to conditions that are not compatible with the stability of the tunnel (exceeding the maximum permissible values of the convergence tunnel).

In this work the results of an extensive laboratory experimentation on the creep behavior, developed for different curing ages of the specimens and different load entities in relation to the UCS of the material, are reported. It was possible to identify which is the maximum compression stress where no failure of the material under a continuous load over time is observed. In addition, it was possible to derive the recurring trend of deformations over time (creep trend) by varying the curing ages and the stress state applied to the specimens.

The information obtained from the experimentation was then used to understand the effects of the creep phase of the two-component material on the interaction between the support system and the tunnel. In particular, it was possible to evaluate the decrease in the radial load applied to the support system (and, therefore, to the segmental lining) and the increase in the deformations of the tunnel wall. Finally, the application of the above considerations to a real case of a tunnel excavated in Northern Italy in a weakly cohesive ground has allowed to understand how the creep of the two-component material has non-negligible effects on

680 the final stress state induced in the segmental lining and on radial displacements of the
681 tunnel wall.

682 **Acknowledgment**

683 The authors wish to thank Master Builders Solutions by MBCC Group for the permission
684 granted to publish the results and to the reviewers' comments which increased the quality
685 of the manuscript.

686 **Conflict of interests**

687 Authors declare they have no conflict of interest.

688 **References**

689 Arnau, O., Molins, C., Blom, C.B.M., Walraven, J. (2011). Longitudinal time-dependent
690 response of segmental tunnel linings. Tunnelling and Underground Space Technology
691 28(1):98, *10.1016/j.tust.2011.10.002*.

692 Barla, G. (2011). Contributions to the understanding of time dependent behaviour in deep
693 tunnels. Geomech Tunnelling; 4: 255-264.

694 Brown E.T., Bray J.W., Ladanyi B., Hoek E. (1983). Ground response curves for rock
695 tunnels. Journal of Geotechnical Engineering,109, 1, 15-39
696 https://doi.org/10.1061/(ASCE)0733-9410(1983)109:1(15)

697 Cardu, M. and Oreste, P. (2012). Technical-operational comparison between trench-cutters
698 and clam excavators for concrete diaphragm construction in underground works at shallow
699 depths. Int. J. Min. Reclamat. Environ., 26, 3, 217–232.

700 Di Giulio, A.. Bavasso, I., Di Felice, M.. and Sebastiani, D. (2020). A preliminary study of the
701 parameters influencing the performance of two-component backfill grout. Gallerie e Grandi
702 Opere Sotterranee. 133. 11-17.

703 Do N.A., Dias D., Oreste P. (2014). Three-dimensional numerical simulation of mechanized
704 twin stacked tunnels in soft ground, Journal of Zhejiang University: Science A, 15(11):896–
705 913.
706 Do N.A., Dias D., Oreste P., Djeran-Maigre I. (2015a). 2D numerical investigation of
707 segmental tunnel lining under seismic loading. Soil Dynamics and Earthquake Engineering
708 72 (2015): 66-76.
709 Do N.A., Dias D., Oreste P. (2015b). 3D numerical investigation on the interaction between
710 mechanized twin tunnels in soft ground. Environmental Earth Sciences, 73(5):2101–2113.
711 Dusseault. M.B. Fordham. C.J. 1993. Time-dependent behavior of rocks. In Hudson JA. ed.
712 Comprehensive Rock Engineering. Pergamon Press: 119–149.
713 Farmer I.W. and Gilbert M.J. (1981). Time dependent strength reduction of rock salt. Proc.
714 1st Conf. on Mechanical Behaviour of Rock Salt, Pennsylvania State Univ.
715 Flores, A.Q. (2015). Physical and mechanical behavior of a two component cement-based
716 grout for mechanized tunneling application. MSc Thesis. Universidade Federal do Rio de
717 Janeiro. Brazil.
718 Geymayer, H.G. (1970). The effect of temperature on creep of concrete: a literature review.
719 U.S. Army Engineer Waterways Experiment Station Corps of Engineers, Vicksburg,
720 Mississippi.
721 Goodman, R. (1980). Introduction to Rock Mechanics. New York: Wiley.
722 Griggs, D. (1939). Creep of rocks. The Journal of Geology, 47, 3, 225-251.
723 Hardy H.R., Kim R.Y., Stefanko R. and Wang Y.J. (1969). Creep and microseismic activity
724 in geologic materials. Proc. 13th US Rock Mech. Symp., Berkeley, 377-413.
725 Hirata, T. (1989). Study on behavior of cohesive soil in type shield tunneling work and on
726 construction technique. Doctoral Thesis. Kyoto University. Japan.
727 Huber, H.G. (1991). Untersuchung zum Verformungsverhalten von jungem Spritzbeton im
728 Tunnelbau. Master Thesis. University of Innsbruck. Austria.

729 Jaeger, J.C.. Cook. N.G.W. (1979). Fundamentals of Rock Mechanics. London: Chapman
730 and Hall.
731 Kuwajima, F.M. Early age properties of the shotcrete. In Shotcrete for Underground VIII.
732 Celestino. T.B. and Parker. H.W.. eds.. Conference Eighth International Conference. São
733 Paulo. Brazil, April 11-15. 1999. American Society of Civil Engineers. Reston. VA.
734 Lama R.D. and Vutukuri V.S. (1978). Handbook on mechanical properties of rock. Testing
735 techniques and results. Vol. III, Trans Tech Publ.
736 Li., J., Sun. G., Zou, H., Zhou, Z., Fan, X. (2019). Influence of temperature and load on creep
737 characteristics of soft rock similar materials. IOP Conf. Series: Earth and Environmental
738 Science 384, 012229, doi:10.1088/1755-1315/384/1/012229.
739 Melbye, T. (1994). Sprayed Concrete for Rock Support. Switzerland: MBT Underground
740 Construction Group.
741 Ochmański, M.. Modoni, G. and Bzówka, J. (2018). Automated numerical modelling for the
742 control of EPB technology. Tunnelling and Underground Space Technology 75. 117–128.
743 *https://doi.org/10.1016/j.tust.2018.02.006*.
744 Ochmański, M., Modoni. G. and Spagnoli, G. (2021). Influence of the annulus grout on the
745 soil-lining interaction for EBP tunneling. Geotechnical Aspects of Underground Construction
746 in Soft Ground: Proceedings of the Tenth International Symposium on Geotechnical Aspects
747 of Underground Construction in Soft Ground, IS-Cambridge 2022, Cambridge, United
748 Kingdom, 27-29 June 2022, 350-356, DOI: *10.1201/9780429321559-45*
749 Oggeri, C.. Oreste, P.. and Spagnoli, G. (2021). The influence of the two-component grout
750 on the behaviour of a segmental lining in tunnelling. Tunnelling and Underground Space
751 Technology. 109. 103750. *https://doi.org/10.1016/j.tust.2020.103750*.
752 Oh, J.Y. and Ziegler, M. (2014). Investigation on influence of tail void grouting on the surface
753 settlements during shield tunneling using a stress-pore pressure coupled analysis. KSCE
754 Journal of Civil Engineering. 18(3). 803-811. DOI: *10.1007/s12205-014-1383-8*.

Oreste P. (2003). Analysis of structural interaction in tunnels using the covergence–confinement approach, Tunnelling and Underground Space Technology, 18, 4, 347-363.

Oreste, P. (2007). A numerical approach to the hyperstatic reaction method for the dimensioning of tunnel supports. Tunnelling and Underground Space Technology 22(2):185–205. https://doi.org/10.1016/j.tust.2006.05.002.

Oreste P (2009a). The convergence-confinement method: roles and limits in modern geomechanical tunnel design. American Journal of Applied Sciences 6(4):757-771.

Oreste P (2009b). Face stabilisation of shallow tunnels using fibreglass dowels. Proceedings of the Institution of Civil Engineers-Geotechnical Engineering, 162(2):95-109.

Oreste P. (2013). Face stabilization of deep tunnels using longitudinal fibreglass dowels. International Journal of Rock Mechanics and Mining Sciences, 58:127-140.

Oreste P (2015). Analysis of the interaction between the lining of a TBM tunnel and the ground using the convergence-confinement method. American Journal of Applied Sciences 12(4):276-283. DOI: 10.3844/ajassp.2015.276.283.

Oreste P., Spagnoli G., Ceravolo LA (2019) A numerical model to assess the creep of shotcrete linings. Proceedings of the Institution of Civil Engineers – Geotechnical Engineering. 172. 4. 344-354. *https://doi.org/10.1680/jgeen.18.00089*.

Oreste, P., Spagnoli, G., Luna Ramos, C.A. (2020). Evaluation of the safety factors of shotcrete linings during the creep stage. Proceedings of the Institution of Civil Engineers – Geotechnical Engineering. 173. 3. 274-282. *https://doi.org/10.1680/jgeen.19.00104*

Oreste, P., Sebastiani, D., Spagnoli, G., de Lillis, A. (2021) Analysis of the behavior of the two-component grout around a tunnel segmental lining on the basis of experimental results and analytical approaches. Transportation Geotechnics, 29, 100570, *https://doi.org/10.1016/j.trgeo.2021.100570*

779 Orumchi, H. and Mojallal, M. (2017). Shear Strength Design of a Mechanized Tunneling
780 Grout Mix: Case Study of the Tehran Subway Line 6 Project. Transp. Infrastruct. Geotech.
781 4, 18–36. *https://doi.org/10.1007/s40515-017-0037-7*
782 Osgoui, R., and Oreste, P. (2007). Convergence-control approach for rock tunnels
783 reinforced by grouted bolts, using the homogenization concept. Geotechnical and
784 Geological Engineering 25(4):431-440, DOI: *10.1007/s10706-007-9120-0*.
785 Panet, M. (1995). Calcul des Tunnels par la Mdthode de ConvergenceConfinement. Paris:
786 Press de l'Ecole Nationale des Ponts et Chausses.
787 Pelizza S., Oreste P., Peila D., Oggeri C. (2000). Stability analysis of a large cavern in Italy
788 for quarrying exploitation of a pink marble. Tunnelling and Underground Space Technology,
789 15(4):421–435.
790 Price A.M. and Farmer I.W. (1981). The Hvorslev surface in rock deformation. Int. Journ. Of
791 Rock Mech. And Min.Sci., 18, 229-34.
792 Ranjbarnia M., Fahimifar A., Oreste P. (2014). A simplified model to study the behavior of
793 pre-tensioned fully grouted bolts around tunnels and to analyze the more important
794 influencing parameters. Journal of Mining Science 50(3):533-548
795 Ranjbarnia, M., Fahimifar, A., Oreste, P. (2016). Practical method for the design of
796 pretensioned fully grouted rockbolts in tunnels. International Journal of Geomechanics,
797 16(1), 04015012
798 Rahmati, S., Chakeri. H., Sharghi. M., Dias, D. 2021. Experimental study of the mechanical
799 properties of two-component backfilling grout. Proceedings of the Institution of Civil
800 Engineers - Ground Improvement. *https://doi.org/10.1680/jgrim.20.00037*.
801 Rokahr, R.B. Lux, K.H. (1987). Einfluss des rheologischen Verhaltens des Spritzbetons auf
802 den Ausbauwiderstand. Felsbau. 5:11-18.

803 Shah, R.. Lavasan, A.A. , Peila. D., Todaro. C., Luciani. A. and Schanz, T. (2018). Numerical
804 study on backfilling the tail void using a two-component grout. J. Mater. Civ. Eng.. 30(3):
805 04018003.
806 Sharghi, M. , Chakeri, H. , Afshin. H. , and Ozcelik, Y. 2018. An experimental study of the
807 performance of two-component backfilling grout used behind the aegmental lining of a
808 Tunnel-Boring Machine. Journal of Testing and Evaluation. 46. 5. 2083–2099.
809 *https://doi.org/10.1520/JTE20160617*.
810 Spagnoli G. Oreste P. Lo Bianco L. (2016). New equations for estimating radial loads on
811 deep shaft linings in weak rocks. International Journal of Geomechanics 16(6): 06016006.
812 DOI: *10.1061/(ASCE)GM.1943-5622.0000657*.
813 Spagnoli G., Miedema S.A., Herrmann, C., Rongau J., Weixler, L. Denegre J. (2016)
814 Preliminary Design of a Trench Cutter System for Deep-Sea Mining Applications Under
815 Hyperbaric Conditions. IEEE Journal of Oceanic Engineering 41, 4, 930 – 943,
816 *10.1109/JOE.2015.2497884*.
817 Thewes, M. and Budach, C. (2009). Grouting of the annular gap in shield tunnelling-An
818 important factor for minimisation of settlements and production performance. Proceedings
819 of the ITA-AITES World Tunnel Congress 2009 “Safe Tunnelling for the City and
820 Environment”. pp. 1–9.
821 Thomas, A. (2009). Sprayed concrete lined tunnels. Oxon: Taylor and Francis.
822 Todaro. C., Peila. L., Luciani. A., Carigi. A.. Martinelli, D. and Boscaro, A. (2019). Two
823 component backfilling in shield tunneling: laboratory procedure and results of a test
824 campaign. In Proceedings of the WTC 2019 ITA-AITES World Tunnel Congress (WTC
825 2019). May 3-9. 2019. Naples. Italy. Peila. D.. Viggiani. G. and Celestino. T. (eds). CRC
826 Press. Boca Raton.

827 Van der Schyff J.J. (2017). Quantifying the creep behaviour of polyester resin and grout.
828 Proceedings of the 17th Coal Operators' Conference, Mining Engineering, University of
829 Wollongong.
830 Yin, J. (1996). Untersuchungen zum zeitabhängigen Tragverhalten von tiefliegenden
831 Hohlraumen im Fels mit Spritzbeton. PhD Thesis. Clausthal University of Technology.
832 Germany.
833 Yu, C.W. 1998. Creep characteristics of soft rock and modelling of creep in tunnel:
834 determination of creep characteristics of soft rock and development of non-linear creep
835 analysis code for squeezing tunnel problem. PhD Thesis. University of Bradford. UK.